LUND UNIVERSITY

New tools for probing biological extremes of ionizing radiation

Nilsson, Charlotta

2008

New tools for probing biological extremes of ionizing radiation

Doctoral Thesis

Charlotta Nilsson

Division of Nuclear Physics
Department of Physics
Lund University
2008

Lunds universitet
Lunds Tekniska Högskola

Akademisk avhandling som för avläggande av teknologie doktorsexamen vid Lunds universitets tekniska fakultet, offentligen kommer att försvaras i föreläsningssal B på Fysiska institutionen i Lund, fredagen den 12 december 2008, kl. 13.15. Fakultetsopponent är Prof. Borivoj Vojnovic, Gray Cancer Institute, Oxford, Storbritannien.

New tools for probing biological extremes
of ionizing radiation

Printed in Sweden by Mediatryck, Lund, 2008

Division of Nuclear Physics
Department of Physics
Lund University
Box 118
S-221 00 Lund
Sweden

ISBN 978-91-628-7646-3
ISRN LUTFD2/(TFKF-1037)/1-78/(2008)

Abstract

Three different biological extremes of irradiation of living organisms, both human and animal, have been investigated and are presented in this thesis. Central to the thesis is the concept of bystander effects of ionizing radiation, i.e. biological responses in a cell that are not caused by that cell receiving a direct hit by ionizing radiation but by the fact that a neighbouring cell has been hit by ionizing radiation. The first extreme is represented by preparations for a single-ion hit facility, providing the opportunity to deliver very low doses, down to single ions, of irradiation with a proton microprobe. Such a facility is a very helpful tool when studying low-dose effects, such as bystander effects, in a well-defined and controlled manner. These preparations consisted of: 1) characterization of thin semiconductor detectors that could be used to detect single ions, and 2) fabrication of a patterned cell substrate, where cells can be guided to grow in small, separated islands.

The second extreme is represented by low-dose experiments on human cells in the search for bystander effects of ionizing radiation. These biological experiments, where a collimated alpha particle source was used instead of a proton microprobe, were carried out on cells cultured in standard Petri dishes. The third and final extreme is represented by irradiation experiments carried out on an extremely radiation-tolerant animal, the tardigrade, illustrating the delivery of very high doses using a proton microprobe — this project being the opposite of the first and second extreme in a sense.

These three projects have resulted in a possible new detector set-up, where a thin transmission detector has been shown to be suitable for use in a single-ion hit facility, and a patterned cell substrate that is easy and fast to fabricate and which is well-suited for irradiation experiments. Furthermore, a protein, α_1-microglobulin, has been shown to have cell-protection properties, minimizing the spread of cell death to bystander cells after alpha particle irradiation. Finally, the tolerance of the tardigrade to proton irradiation has been investigated for the first time, revealing that this animal is indeed extremely radiation tolerant.

Populärvetenskaplig sammanfattning

Alla levande varelser, människor såväl som djur, utsätts under hela sin livstid för en låg konstant bestrålning — denna kallas bakgrundsstrålning. Bakgrundsstrålningen, som bland annat kommer från radon i hus och mark, kosmisk strålning, radioaktiva ämnen i kroppen samt medicinska undersökningar och behandlingar, uppgår till cirka 4 milliSievert (mSv) per år. Denna dos är avsevärt mycket mindre än de doser som hittills med säkerhet visats vara skadliga. De data som finns gällande samband mellan stråldosen och de biologiska effekterna av strålningen — den s.k. responsen — kommer framför allt från studier gjorda på överlevande från atombomberna i Hiroshima och Nagasaki samt efter haveriet i kärnkraftverket i Tjernobyl. Man har exempelvis sett en ökad frekvens av antalet cancerfall, framför allt leukemi, hos överlevande från Hiroshima och Nagasaki. Vid dessa höga strålningsdoser råder ett linjärt samband mellan dos och respons. Om detta linjära samband också är giltigt vid mycket lägre doser, motsvarande bakgrundsstrålningen, är ännu inte klarlagt. Tidigare har man antagit ett linjärt samband även för dessa lägre doser, men alternativa teorier finns. Exempelvis finns en teori kallad "low-dose hypersensitivity" — enligt vilken en mycket låg stråldos skapar oproportionerligt stor skada. Samtidigt finns en annan teori — "Hormesis" — där det motsatta hävdas; att låga stråldoser i själva verket skulle vara hälsosamma.

Denna avhandling belyser några olika aspekter som rör experiment där enskilda levande celler utsätts för låga stråldoser. Avhandlingen är uppbyggd av tre olika delar, som var och en representerar någon extrem vad gäller biologiska effekter av strålning. Den effekt som avhandlingen framförallt fokuserar på kallas för "bystander"-effekt. Den innebär att en cell kan uppvisa biologiska effekter av strålning, även om cellen inte träffats direkt av någon strålning. Cellen i fråga kan reagera som om den själv utsatts för bestrålning, trots att det är en närliggande cell som bestrålats. Låga stråldoser kan med fördel studeras med hjälp av acceleratorer, som anpassats för att möjliggöra bestrålning av levande prover. Den första delen av avhandligen behandlar några av de

acceleratoranpassningar som behöver göras — nämligen en undersökning av en typ av detektor som passar att placeras framför, istället för bakom, cellerna i en experimentuppställning för lågdosförsök och också utvecklingen av en mönstrad cellskål som möjliggör odling av celler i olika mönster, något som kan underlätta studier av "bystander"-effekter. Nästa del behandlar biologiska bestrålningsförsök som gjorts på levercancerceller som odlats i vanliga Petriskålar. En liten andel av cellerna i skålen bestrålades med alfapartiklar, d.v.s. heliumkärnor, medan övriga celler i skålen inte utsattes för någon strålning. När andelen döda celler, dels bland dem som bestrålats, dels bland övriga, ej direkt bestrålade, celler, i skålen undersöktes, blev det tydligt att inte bara de direkt bestrålade cellerna utan även deras grannceller i skålen påverkats av strålningen. I försöken har ett protein, som antogs ha egenskapen att skydda celler från effekter av strålning, undersökts — med lovande resultat. Proteinet visade sig kunna skydda såväl direkt bestrålade celler som grannceller mot effekter av strålning, så att andelen döda celler minskade kraftigt. Den sista delen av avhandlingen berör försök gjorda på ett utomordentligt strålningståligt litet djur, björndjuret (tardigrada). Försöken visar att björndjuret klarar av ungefär 1000 gånger högre stråldoser än en människa.

List of publications

This thesis is based on the work behind the following publications, which will be referred to in the thesis by their roman numerals. The publications are listed here together with the contribution of the author. The papers are appended at the end of the thesis.

Paper I

Evaluation of a pre-cell hit detector for the future single ion hit facility in Lund
E.J.C. Nilsson, J. Pallon, G. Thungström, N. Arteaga, V. Auzelyte, M. Elfman, P. Kristiansson, C. Nilsson, M. Wegdén
Nuclear Instruments and Methods in Physics Research B **249** (2006) 924-927
Proceedings of the 17th International Conference on Ion Beam Analysis

I planned and carried out the experiment, analysed the data and wrote the paper.

Paper II

Characterisation of a pre-cell hit detector to be used in single cell irradiation experiments at the Lund Nuclear Microprobe
E.J.C. Nilsson, J. Pallon, G. Thungström, N. Arteaga Marrero, M. Elfman, P. Kristiansson, C. Nilsson, M. Wegdén
Nuclear Instruments and Methods in Physics Research B **266** (2008) 4808-4815

I planned and carried out the experiment, analysed the data and wrote the paper.

Paper III

Using microdispensing to manufacture a customized cell dish for microbeam irradiation of single, living cells
E.J.C. Nilsson, M.G. Olsson, J. Nilsson, J. Pallon, A. Masternak, J. Pacznesky, N. Arteaga Marrero, M. Elfman, P. Kristiansson, C. Nilsson, B. Åkerström
Submitted to Nuclear Instruments and Methods in Physics Research B

I designed and manufactured the cell dishes, performed the PIXE analysis, analysed the PIXE data and wrote the paper.

Paper IV

The lipocalin α_1-microglobulin inhibits spreading of cell death in alpha-particle irradiated HepG2-cells
M.G. Olsson, J. Pacznesky, E.J.C. Nilsson, J. Pallon, B. Åkerström
Manuscript

I took part in the planning of the irradiation experiments, executed the dose calculations, carried out the irradiations and wrote a minor part of the paper.

Paper V

Tolerance to proton irradiation in the eutardigrade *Richtersius coronifer* — a nuclear microprobe study
E.J.C. Nilsson, K.I. Jönsson, J. Pallon
Manuscript

I planned and carried out the irradiations, executed the dose calculations, performed the PIXE and STIM analysis, analysed the PIXE and STIM data and wrote the paper together with Ingemar Jönsson.

The published papers are reprinted with the kind permission of the copyright holder and their cooperation is gratefully acknowledged.

Elsevier B.V.
Radarweg 29
1043 NX Amsterdam
The Netherlands

Related publications not included in the thesis

Status of the new Single-Ion Hit Facility for Irradiation of Single Living Cells at LIPSION
E.J.C. Nilsson, S. Petriconi, T. Reinert, T. Butz
Radiation Research **166** (4) (2006) 672-673
Extended abstract, Proceedings of the 7th International Workshop: Microbeam Probes of Cellular Radiation Response

The new target chamber at LIPSION: The new translation stage and goniometer and the new irradiation platform for single cell experiments
E.J.C. Nilsson, S. Petriconi, T. Reinert, T. Butz
Nuclear Instruments and Methods in Physics Research B **260** (2007) 71-76
Proceedings of the 10th International Conference on Nuclear Microprobe Technology and Applications

Applications of SU-8 in the development of a Single Ion Hit Facility
N. Arteaga-Marrero, G. Astromskas, M.G. Olsson, M. Elfman, P. Kristiansson, E.J.C. Nilsson, C. Nilsson, J. Pallon
Accepted for publication in Nuclear Instruments and Methods in Physics Research B
Proceedings of the 11th International Conference on Nuclear Microprobe Technology and Applications

First results from the Lund NMP particle detector system
P. Golubev, P. Kristiansson, N. Arteaga-Marrero, M. Elfman, K. Malmqvist, E.J.C. Nilsson, C. Nilsson, J. Pallon, M. Wegdén
Accepted for publication in Nuclear Instruments and Methods in Physics Research B
Proceedings of the 11th International Conference on Nuclear Microprobe Technology and Applications

STIM evaluation in GeoPIXE to complement the quantitative Dynamic Analysis
J. Pallon, C.G. Ryan, N. Arteaga Marrero, M. Elfman, P. Kristiansson, E.J.C. Nilsson, C. Nilsson
Accepted for publication in Nuclear Instruments and Methods in Physics Research B
Proceedings of the 11th International Conference on Nuclear Microprobe Technology and Applications

Contents

Chapter 1

Introduction

1.1 Background

In everyday life, all living beings, humans as well as all other species, are exposed to ionizing radiation. Radiation to humans is composed of contributions from natural as well as artificial sources. Natural sources of radiation include cosmic radiation, radioactive substances in the body (e.g. ^{40}K and ^{14}C) and radiation from radioactive substances in the surroundings, e.g. in the ground and the air, as well as in concrete. The artificial sources are mainly radiation from nuclear power generation, radioactive emissions/pollutants and (atmospheric) nuclear weapons tests and, of course, the fraction from medical treatment such as X-ray examinations and diagnostic and therapeutic procedures in cancer treatment.

Compared to certain other species, human beings are not very tolerant to ionizing radiation — the 50 % lethal full-body dose (LD50) for a human is about 4 Gy. This can be compared with the doses tolerated by other animals, such as dogs (LD50 = 3.7 Gy), mice (7 Gy) and rhesus monkeys (5.25 Gy) [1]. Perhaps the most radiation-tolerant species of all are the millimetre-sized invertebrate tardigrades, whose LD50 dose is about 6000 Gy, i.e. about 1000 times that for humans. However, little is known about why these animals are so radiation tolerant — open questions are for example whether or not they suffer DNA damage and, if so, how efficient their DNA repair mechanisms are.

Most of our knowledge about radiation-induced damage to humans gathered so far is based on accidents, e.g. Chernobyl, and atomic bomb survivors. In these high-dose cases, where the doses received lie in the range 50-2500 mGy, the dose-response curve (e.g. for cancer rates) shows a linear dependence. Based on these data, the linear no-threshold (LNT) model for dose-response when exposed to ionizing radiation is today believed to be valid. However,

there is an ongoing debate on the validity of the LNT model in cases of low doses — below 200 mGy [2, 3], and down to a single ion. Other theories that are being discussed are a linear threshold model, a radiation hormesis model — according to which, background levels of radiation are actually beneficial to humans — and a low-dose hypersensitivity model — according to which, a very low dose can be disproportionately harmful.

Research in the field of cellular response to low-dose radiation has been in progress since the 1950s. Initially, the radiation experiments on different cell cultures were mainly directed towards medium transfer experiments and broad-beam irradiation experiments. Over the past two decades, starting with work done at RARAF, Columbia University in New York, US [4] and at the Gray Cancer Institute (GCI) in Northwood, UK [5], charged particle microbeams have been utilized to irradiate single cells with single MeV energy ions in a well-defined manner — with a lateral resolution of a few μm. Following these early pioneers, several research groups in Europe, Japan and the USA have been and still are developing single-ion hit facilities (SIHFs) for the irradiation of single, living cells [6, 7].

The advantage of microbeam irradiation as opposed to broad-beam irradiation is the possibility of targeting individual cells with a well-defined dose, instead of a random, Poisson-distributed dose to a specific cell. Targeting a specific cell in a culture also provides the opportunity to study the effects on neighbouring cells, that surround the irradiated cell, but have not received any direct irradiation. The effects exhibited by these un-irradiated neighbour cells are usually gathered under the generic term "bystander effects" [8]. In 2004, ten European universities and research facilities formed in 2004 an EU supported Marie Curie Research Training Network, CELLION [9], to carry out "Studies on cellular response to targeted single ions using nanotechnology", to investigate this phenomenon in more detail.

1.2 Outline of this thesis

The work presented in this thesis is a combination of three different projects that illustrate three different extremes in the irradiation of living organisms, both human and animal. These are in turn preparations for a single ion hit facility, biological experiments on human cells in search of bystander effects and irradiation of tardigrades, "water bears", with very high doses — representing low doses, down to single ions, using a proton microprobe, low doses using a collimated alpha particle source and very high doses using a proton microprobe, respectively.

The first and third projects are related in that they are both concerned with proton irradiation using a nuclear microprobe, the first at very low doses in a SIHF and the second at very high doses delivered to radiation-tolerant

tardigrades. The first and the second project are connected in that they both deal with low doses of ionizing irradiation to living human cells. Finally, the second and the third projects have in common that they both represent the more biological, applied part of this research, in contrast to the mainly technical first part.

The first project has in part been carried out within the framework of the EU project CELLION. The purpose of this part of my research was to investigate two aspects of the preparations that are needed in order to assemble a SIHF for irradiation of single, living cells, as well as to develop some of the tools required. The first three papers deal with the issues of single-ion hit detection and guided cell growth. The initial focus of these studies was on the development of a single-ion hit detection system to be positioned in front of the cell dish. This work was centred around investigations of transmission detectors suitable for use in external-beam experiments — the work is presented in Papers I and II and in Chapter 5. Work on a patterned cell substrate for guided and restricted cell growth, well-suited for biological investigations of low-dose effects including bystander effects, then followed — this work is presented in Paper III and Section 6.1. Actual biological investigations of the bystander effect are presented in Section 6.2 and in Paper IV. Finally, the third part of this research, which is presented in Paper V and Chapter 7, deals with the other radiation extreme — it is a study of survival following very high doses of proton irradiation in the extremely radiation-tolerant species Tardigrada.

This thesis is divided into seven main chapters. In Chapters 2-4, a general background to physical and biological effects of ionizing radiation as well as a general description of a single ion hit facility are given. In the following three chapters, I wanted to provide the reader with complementary information on, and pictures from, the experiments that were carried out — data that was not possible to fit into the papers. The actual results of the experiments are, on the other hand, described in detail in the respective papers. Chapter 5 serves as a complement to Papers I and II, including extra information on the experimental procedure, and covers the search for a pre-cell detector. In Chapter 6, which covers both the preparation of patterned cell substrates as well as irradiation experiments on cells, a large set of images, which was beyond the scope of Papers III and IV, is presented along with some more background. In Chapter 7, a description of the biology of the Tardigrada is given, as well as data complementary to the results shown in Paper V.

Chapter 2

Physical effects of ionizing radiation

2.1 Interaction of charged particles with matter

When charged particles, ions, pass through matter they undergo the following two changes: 1) energy loss, or stopping and 2) deflection from their incident direction, or straggling. These effects are the result of two main processes — inelastic collisions with the atomic electrons of the material and elastic scattering from the nuclei [10]. In the case of light nuclei, e.g. protons and alpha particles, inelastic collisions with electrons are almost exclusively responsible for the energy loss of the ions as they travel through matter. Each collision will result in a very small fraction of the ion's energy being transferred to the atom, causing either excitation or ionization of the atom. The atomic collisions that lead to excitation are known as soft collisions while those that cause ionization of the atom are called hard collisions. In some hard collisions, the energy transfer to the electron is so great that the electron itself can be responsible for significant secondary ionization. In these cases, high-energy recoil electrons called δ-rays are created, sometimes even perpendicular to the direction of the incoming ion. An ion track can be said to consist of a "core" region and a "penumbra" region — the core region can be described by the maximum extension of the excitations caused by the primary particle, usually less than 10 nm, and the penumbra region can be described by the maximum distance covered by the secondary electrons [11].

These δ-rays should not be neglected when considering the biological effects of single ion tracks through cells. The common way of estimating the number of particle traversals per cell, T, i.e. by multiplying the area of the cell A_{cell} by the number of ions per unit area (fluence), F:

$$T = F \times A_{cell} \tag{2.1}$$

may not be accurate, as it does not take into consideration the secondary electrons that contribute to the finite width of the ion's track. In the case of high-charge and high-energy particles, the cross-sectional area of the track may be orders of magnitude greater than the cross-sectional area of the cell, a fact that may have implications when studying the bystander effect. To determine whether or not the finite width of the track, i.e. the contribution of the secondary electrons, will affect the number of particle-track traversals per cell, the concept of radial dose, i.e. the average radial distribution in ionization, including a radial dose cutoff value, D_{cut}, can be used to define the effective area of a particle track [11]. The effective cross-sectional area A_{track} can then be defined as:

$$A_{track} = \pi \times (r_{track} + r_{cell})^2 \tag{2.2}$$

where r_{track} and r_{cell} are the radii of the track at the cut-off and of the cell, respectively. For small values of r_{track}, A_{track} will be reduced to A_{cell} — which is the LET (linear energy transfer) approximation. When this approximation does not apply, A_{track} will depend on the velocity and charge of the ion as well as on D_{cut}.

In the situation discussed in this thesis, irradiation with alpha particles with an LET of about 100 keV/μm, the difference between the LET approximation and the value obtained using the radial dose cut-off D_{cut}, is negligible [11]. In other words, the number of adjacent cells that should have been traversed by the deposition of energy corresponding to D_{cut} by δ-rays as the result of one direct ion traversal of a cell, does not have to be taken into account. For heavier ions, such as uranium, iron or even carbon, the discrepancy is, however, pronounced. The way in which the beam damage spreads outside the beam diameter is known as the proximity effect. MeV protons deposit their energy within a nanometre radius, thus the proximity effect is very small [12].

In matter of normal density, the number of inelastic collisions per unit path length is large, meaning that the ion will lose all its energy over a relatively short distance — typical values of the range of 2.55 MeV protons are 114 μm, 71 μm and 107 mm in water, silicon and air respectively. Figures 2.1 and 2.2 show a comparison between 8 MeV alpha particles and 2 MeV protons as they penetrate 100 μm water (equivalent to about 10 cell layers). The figures were produced using the simulation software Stopping and Range of Ions in Matter, SRIM, [13].

The average energy loss per unit path length is known as the stopping power, expressed dE/dx, and it is known to vary with the energy of the particle, as well as with the particle type. Some typical curves can be found in Figure 2.3.

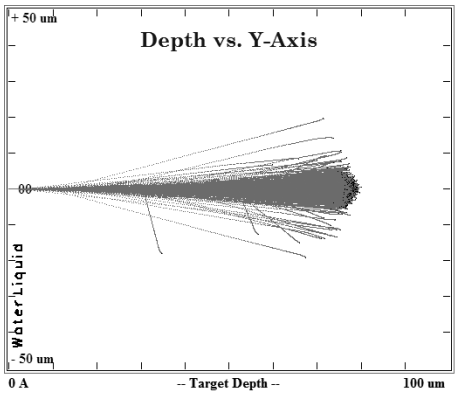

Figure 2.1: Beam straggling and range of 8 MeV α particles in water.

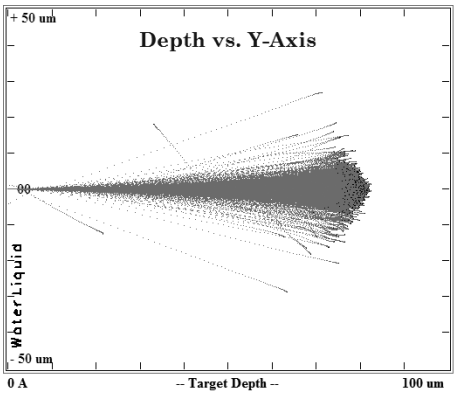

Figure 2.2: Beam straggling and range of 2 MeV protons in water.

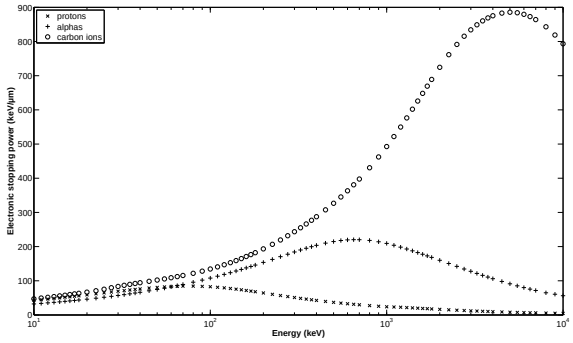

Figure 2.3: dE/dx_{elec} as a function of energy for protons, alpha particles and carbon ions in water.

As mentioned above, the electronic stopping power dominates over the nuclear stopping power. For a 2 MeV proton in water, the electronic stopping power is 16.42 keV/μm, while the nuclear stopping power is 1.14×10^{-2} keV/μm, and for an 8 MeV alpha particle, the electronic and nuclear stopping powers are 65.05 keV/μm and 4.63×10^{-2} keV/μm, respectively. Electronic and nuclear stopping power curves for protons in water are shown in Figure 2.4. As a charged particle, such as a proton or an alpha particle, penetrates matter, the particle's rate of energy loss will thus change as its kinetic energy changes. Even more importantly, it is evident that more energy per unit path

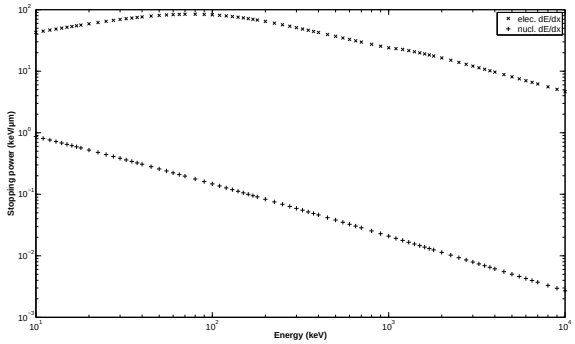

Figure 2.4: dE/dx_{elec} and dE/dx_{nucl} as a function of energy of protons in water.

length will be deposited at the end of the particle's path than at the beginning. This is demonstrated in Figure 2.5, where the Bragg curves for a few different particles are shown as they penetrate 200 μm of water, resembling a biological sample.

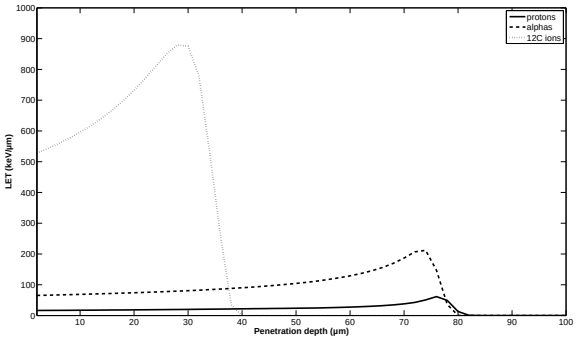

Figure 2.5: Bragg curves, showing LET as a function of penetration depth in water, for protons (solid line), α particles (dashed line) and C ions (dotted line) — all particles have an initial energy of 2 MeV/nucleon, i.e. the same velocity.

Directly ionizing radiation

All charged particles, such as electrons, protons and alpha particles as well as heavy ions, that encounter a target, e.g. a biological sample, are capable of directly ionizing the atoms in the target as they penetrate. They will directly remove electrons from the atoms, thus creating ions along their way.

Indirectly ionizing radiation

γ-rays and X-rays are electromagnetic radiation — γ-rays are intra-nuclearly produced photons and X-rays are photons produced extra-nuclearly. γ-rays and X-rays are not charged, and are thus not capable of directly ionizing atoms. However, they can remove electrons from atoms, producing fast-moving charged particles through three processes of interaction — the photoelectric effect, Compton scattering or pair production, thus indirectly ionizing the atoms.

The photoelectric effect: If a photon encounters a bound electron in an atom, the photon will give up all its energy to the electron, which, due to this sudden increase in energy, will leave its orbit around the atom — thus, the atom becomes ionized.

Compton scattering: If a photon encounters a "free" electron, i.e. an electron in an outer electron shell, the photon and that electron will collide in a billiard-ball-like fashion and scatter, a process during which the electron receives some of the photon's energy.

Pair production: Provided a photon has sufficient energy, it can form an electron-positron pair.

2.2 Ion beam analysis

A beam of ions that interacts with a sample will produce a wide range of particles (see Figure 2.6) — including scattered ions, characteristic X-rays, Auger and secondary electrons, photons or charged particles from nuclear reactions, and visible light — that can be used to obtain qualitative and quantitative information about the sample, such as elements, isotopes and chemistry. The term ion beam analysis (IBA) covers a collection of analytical techniques, including particle induced X-ray emission (PIXE), Rutherford backscattering spectroscopy (RBS), elastic recoil detection analysis (ERDA) and nuclear reaction analysis (NRA) [14].

Combining a focused charged particle microbeam from an accelerator with other instrumentation, including detectors, a scanning system and a data acquisition system, forms a microanalytical tool — a nuclear microprobe (NMP). This focused ion beam can be utilized to characterize, image and even modify a microscopic sample, such as a single cell. Concentrations of elements can be determined with high sensitivity, and by scanning the beam over the

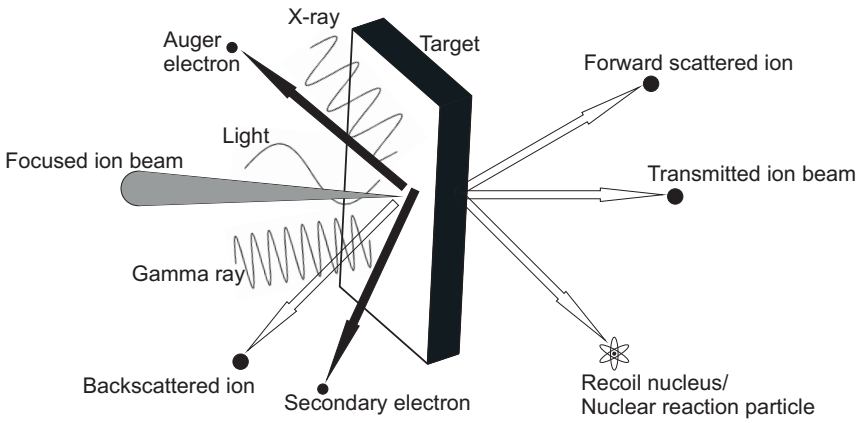

Figure 2.6: Various processes that can occur when an MeV ion beam interacts with matter.

sample, two-dimensional information on the distribution of elements can be obtained with a lateral resolution of a few μm or less. IBA methods are often complementary, and several analysis methods can generally be employed simultaneously.

2.2.1 Scanning transmission ion microscopy

Using the analytical method scanning transmission ion microscopy (STIM) [15], the mass of a sample can be determined. As an ion passes through matter, it will undergo ion-electron interactions, i.e. Coulomb interactions, with the nuclei and electrons in the sample, which will cause the ion to lose energy. By measuring this energy loss — which, for a given ion and energy, depends on the elemental concentration, the mass density and the thickness of the sample — the areal mass density of the sample can be calculated if the stopping power of the material is known. The magnitude of the energy loss will thus give an indication of the thickness of the sample. Figure 2.7 shows a STIM image of two dehydrated water bears.

2.2.2 PIXE

The ion beam analytical method PIXE [16] utilizes the fact that incoming MeV energy ionizing radiation (e.g. protons) causes inner shell ionization of the atoms in the sample. Inner shell electrons in the atom are ejected and outer shell electrons fill the vacancies that arise, and in doing so they emit X-rays,

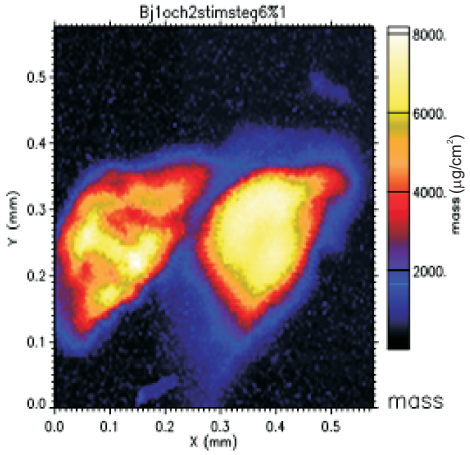

Figure 2.7: STIM image of two dehydrated tardigrades.

i.e. eV-keV energy photons, (or in some cases Auger electrons). As only certain transitions are allowed, the energy of the X-rays emitted is characteristic of the atom that has been ionized. Each element has its own series of characteristic X-rays, originating in the different electron shells. Transitions to the K-shell from the L-shell are called K_α, those from the M-shell to the K-shell are called K_β, and analogously for the other transitions; L_α, M_α etc.

By measuring the characteristic X-rays using an energy-dispersive detector, the PIXE method offers the possibility of qualitative as well as quantitative elemental analysis of samples of unknown composition. Elements heavier than magnesium can be detected — the lightest elements of the periodic table cannot be detected, since their characteristic X-rays are too soft, i.e. have too low an energy, to be registered in the detector. PIXE analysis can be combined, even simultaneously, with other ion beam analysis methods, such as RBS, to quantify all elements.

The method is non-destructive, making it suitable for a wide range of sensitive and/or valuable samples. Further advantages are that PIXE is a multi-element method, i.e. many elements can be analysed simultaneously, and that the sensitivity is high compared with traditional methods such as X-ray fluorescence and the electron microprobe (EMP). Furthermore, low concentrations ($<$ppm) can be analysed [17]. Also, PIXE allows for quantitative analysis without using standards [18]. In Figure 2.8 a typical PIXE spectrum is shown,

depicting a dehydrated water bear.

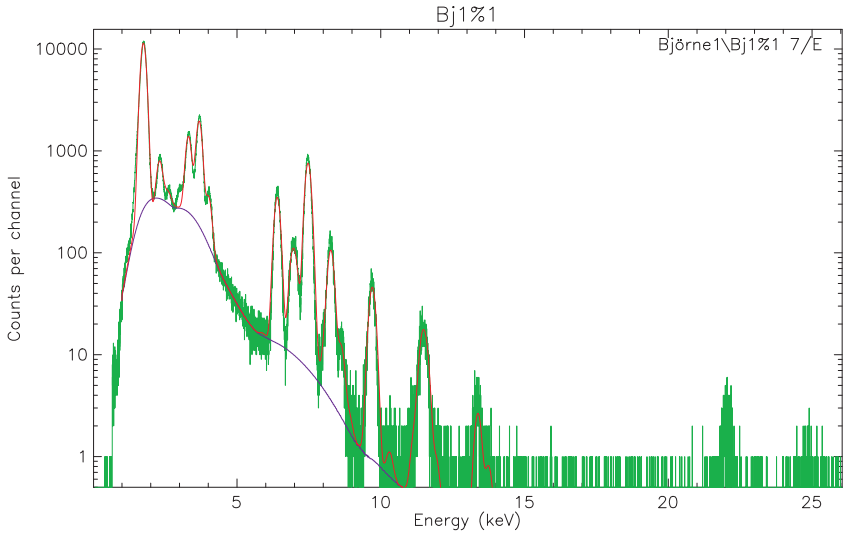

Figure 2.8: A PIXE spectrum of a dehydrated tardigrade.

Compared with other microprobe techniques, such as the electron microprobe, the detection limit of the nuclear microprobe is 2-3 orders of magnitude better — mg/g in the case of an electron microprobe can be compared with ppm levels in the case of a nuclear microprobe. The background in an X-ray spectrum obtained using electron-induced X-ray emission is far more intense and extends to higher X-ray energies than the background in a PIXE spectrum, due to the fact that electrons are scattered much more than protons (or other heavier particles), giving rise to much more bremsstrahlung radiation (the background in the PIXE spectrum is due to secondary electron bremsstrahlung). The spatial resolution, on the other hand, is better in electron microscopy, due to brighter electron sources, and better lenses and simpler beam optics for focusing [14]. The penetration depth is better in the case of a nuclear microprobe with ions having an energy of a few MeV. These ions can penetrate a few tens of micrometres into a specimen, allowing bulk analysis of the surface region.

2.3 The Lund Nuclear Microprobe

As any other NMP, the Lund Nuclear Microprobe consists of four main building blocks: an accelerator, beam lines, target chambers and a data acquisition system. The Lund NMP accelerator is a single-ended 3 MV NEC electrostatic

Pelletron van de Graaff accelerator, equipped with a radio frequency (RF) ion source, placed inside the accelerator's pressure tank. The RF ion source is capable of producing protons, deuterons or alpha particles, which can then be accelerated up to an energy of 3 MeV. The Lund NMP nanoprobe beamline is illustrated in Figure 2.9.

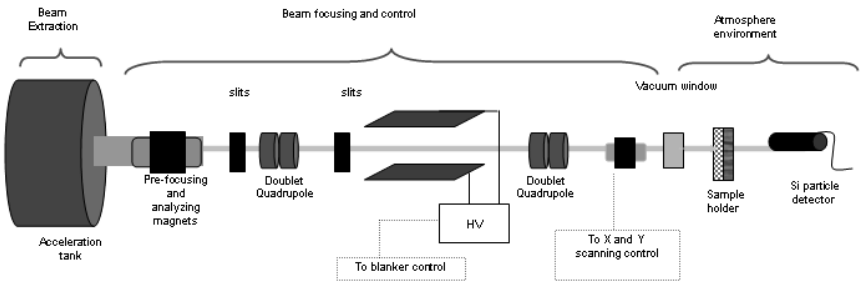

Figure 2.9: Schematic of the Lund NMP nanoprobe beamline, courtesy of Dr. Vaida Auzelyte.

The Lund NMP is a focused, as opposed to a collimated, microprobe, utilizing magnetic quadrupole lenses to focus the MeV ions. Outside the acceleration tank, after the analysing magnet, the NMP is divided into two (previously three) separate operational beam lines, the macro-beam line and the sub-micron (nano) beam line, capable of producing millimetre and sub-micrometre sized beams, respectively. To achieve the desired sub-micrometre beam size, the nano-beam line [19] is equipped with a two-stage magnetic quadrupole focusing system (two separated doublets). Theoretical calculations [20] show that the theoretically attainable beam spot size of the nano beam line is 200 nm $\times$ 500 nm.

Along the beam lines, several magnetic and electrostatic devices, including steerers and beam profile monitors, are responsible for aiding the focusing and steering of the beam. Beam stops and beam viewers assist in beam transport and help in the optimization (control and measurements) of the beam. Object and aperture slits, V-shaped Fischer slits [21], are needed to control the beam size and the beam current, and are controlled by micrometre screws. A fast beam-blanking system, originally installed for use in proton beam lithography [22], will serve as an integral part of the single ion hit facility, enabling the production of single, or a specific number of ions. The target chamber of the nano-beam line [23] is equipped with a detector for traditional PIXE analysis — an annular, large-area (800 mm^2), 8-element HPGe detector [24] — together with Hamamatsu p-i-n diodes for STIM measurements. Non-targeted cell ir-

radiation experiments have been carried out routinely at the Lund NMP since June 2006 [25], and the first successful results on cells experiencing oxidative stress following proton irradiation have been presented [26].

Chapter 3

A single-ion hit facility

A single-ion hit facility, in its simplest form, is composed of three building blocks [27]: a nuclear micro- or nanoprobe, a fast beam blanker/chopper to deflect the beam and a fast detector to detect single-ion hits with almost 100 % efficiency. For the irradiation of living cells, a SIHF must also be equipped with a vacuum window (sometimes called a beam exit window), separating the very low pressure (around 10^{-6} mbar) in the beam line from the atmospheric pressure around the sample stage/irradiation platform where the living cells are kept, through which the ion beam is extracted into the ambient air. The majority of SIHFs for single-cell irradiation that are operational or under development today use light ions (mainly protons or alpha particles). Important exceptions are GSI (Darmstadt, Germany) and JAERI (Takasaki, Japan) where heavy ions are used; at GSI from He to U, often C and Ar, and at JAERI mainly C, Ne and Ar. At SNAKE (Munich, Germany) light as well as heavy ions, from H to Au, often O, can be used at projectiles.

Other options, instead of employing a charged particle microprobe, are X-ray and electron microprobes. A few facilities utilizing either low-energy (ultrasoft) X-rays [28] or low-energy electrons [29, 30] exist today. The X-ray microprobe is at least as favourable as the charged particle microprobe as far as beam size is concerned, as the main mode of interaction of X-rays in the keV range is via the photoelectric effect, so that virtually no scattering takes place, resulting in a minimum beam size of below a micron. The electron microprobe is the least favourable in regard to beam size as the electrons will produce secondary electrons with a long range [3].

3.1 Beam blanker

To have the possibility to control the beam and produce a single ion, or a well-defined number of ions, a fast beam blanker or chopper is needed. Commonly, a fast electrostatic beam blanker or steerer, consisting of two parallel metal plates that are connected to a fast voltage generator, is used [22]. At the Lund NMP, the beam-blanking system was originally implemented as an integral part of the ion beam lithography system, but it is equally important for single-cell experiments and charge measurements [31].

3.2 Ion beam interactions in matter

Beam stopping and beam straggling, as discussed in detail in Chapter 2, both play a crucial role when designing the instrumentation for a SIHF. These effects must be taken into consideration when choosing the single-hit detector and the vacuum window material. Depending on which detection approach is chosen, either the straggling or the stopping can be the main limitation. In choosing the vacuum window material, care must be taken primarily regarding beam straggling. The thicker the layers and the greater the number of layers between the vacuum and the ambient pressure region in which the living cells are irradiated, the more beam energy will be lost. Also, the greater the distance from the first scattering point to the target, the greater the particle's deviation from its incident direction. The software SRIM [13] is a powerful tool for simulating SIHF set-ups with various types of vacuum windows and detectors in different arrangements. In Figure 3.1, the result of a simulation in SRIM is shown, which illustrates the spreading of a 2.55 MeV proton beam as it passes through a 9 μm thick silicon wafer.

3.3 Single-hit detector

There are two options of detecting the ions, either before (pre-cell detection) or after (post-cell detection) they reach the sample. Both methods have advantages as well as disadvantages [32]. Pre-cell detection, on the one hand, allows for additional layers in the Petri dish, e.g. to keep the cells in a hydrated atmosphere, and an arbitrary amount of medium is allowed. However, pre-cell detection suffers from increased, unwanted beam spreading if the detector is placed in the beam, actually obstructing it and causing it to lose energy (e.g. in the case of a scintillating foil). This is, however, not the case if a channeltron detector is used to detect secondary electron emission as the beam passes through the vacuum window. The advantage of post-cell detection is naturally that no additional obstruction of the beam takes place, but the disadvantage

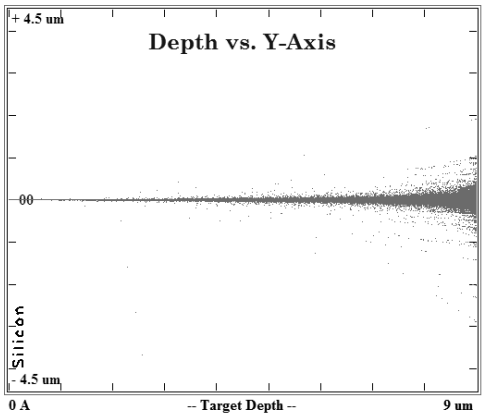

Figure 3.1: 2.55 MeV protons in 9 μm silicon

is that care must be taken to ensure that the beam has enough energy to reach the detector. If it does not, single-ion delivery can not be ensured, and a minimum of medium must thus be used, and no additional layers are allowed in the Petri dish.

When choosing a detector for use in single-ion experiments, especially if it is to be positioned before the ions reach the cell dish, the detector must be able to produce a detectable, useful signal with as little beam energy loss as possible. A certain amount of ionization is required to produce a signal in the detector, and is dependent on the noise in the detector and electronics. Noise is always present, regardless of whether any radiation is present or not, and will appear as a fluctuating voltage or current at the detector output. For the ionization signal to be useful, it must be clearly separated from the noise. Depending on the type of detector chosen, a specific amount of ionization will produce very different numbers of "information carriers", i.e. the particles produced in the ionizing process that are to be collected and serve as detection of the ionizing radiation. In the case of a semiconductor, only 3 eV is needed to form an electron-hole pair; in a gas-filled detector about 30 eV is required to create an ion-electron pair, and in a scintillator around 300 eV is necessary to produce a photon, or scintillation, that can be detected. This means that, for a given energy deposition, a hundred times more information carriers will be produced in a semiconductor detector than in a scintillator. In addition, when using a scintillation detector, the efficiency of the photomultiplier tube is typically about 30 %, i.e. only 30 % of the collected photons will be detected [10].

In photomultipliers, as well as in semiconductors, leakage currents will contribute to the noise. When a voltage is applied to a semiconductor junction, a

small fluctuating current will flow, even if the semiconductor should ideally be nonconducting under these circumstances — this is known as the leakage current. This leakage-current-induced noise at the detector output will set a limit on the minimum pulse amplitude that can be reliably detected. Furthermore, the depletion depth in the semiconductor must be sufficiently thick to ensure that enough ionization will be produced to create a signal that is greater than the noise level. This could be an additional difficulty when using an ultrathin, semiconductor, pre-cell detector.

A detection efficiency as close to 100 % as possible, in practise above 95 % [33], is required to ensure accurate measurement of the delivered dose. Several different types of detectors are used within the single-ion irradiation community: scintillators (together with photomultiplier tubes), gas-filled detectors, semiconductor detectors and channeltrons. In the table below, the detector types and their locations used at some SIHFs for cell irradiation experiments, operational or under construction, are given.

SIHF	Detector type	Detector location
CENBG, Bordeaux	BC 400 scintillator, 7.5 μm or proportional counter (10 mbar, isobutane)	Pre-cell [34]
RARAF, New York	Pulsed ion counter (P10 gas) or Schottky barrier detector, 2 μm Si	Post-cell [35]
GCI, Oxford	BC 400 scintillator, 18 μm	Pre-cell [36]
GSI, Darmstadt	Channeltron	Pre-cell [37]
JAERI, Takasaki	BC 400 scintillator	Post-cell [38]
Krakow	Silicon surface barrier detector	Post-cell [39]
LIPSION, Leipzig	Windowless p-i-n diode	Post-cell [40]
LNL-INFN, Legnaro	Silicon surface barrier detector	Post-cell [41]
Lund NMP	Windowless p-i-n diode	Post-cell [25]
MIT, Boston	Plastic scintillator, 5 μm	Pre-cell [42]
PTB, Braunschweig	BC 400 scintillator, 10-50 μm	Pre-cell [43]
SNAKE, Munich	BC 400 scintillator, 1 mm	Post-cell [44]
Surrey, Guildford		[45]

3.3.1 Semiconductor detectors

The semiconductor detector is one type of detector commonly used in nuclear physics and ion beam analysis experiments, as it is suitable for charged particles as well as γ-rays. A semiconductor detector typically consists of a semiconductor crystal, usually silicon or germanium, with two connectors. When a charged particle passes through the detector, electron-hole pairs are created.

The electrons that are released are excited into the conduction band of the semiconductor, where they become free to move in the crystal. Consequently, they are rapidly collected by the positive electrode. This movement of free electrons in the conduction band is one of the two contributions to the electric current in a semiconductor; the other is the analogous movement of holes in the valence band.

Semiconductor detectors utilize a p-n junction, i.e. two doped semiconductor materials (one n-type and one p-type). At the interface between the two materials, i.e. in the p-n junction, a zone is formed where the excess electrons will initially diffuse toward the p-region and the excess holes will diffuse toward the n-region. This recombination of electrons and holes creates an electric field gradient across the junction, which eventually leads to a cessation of the diffusion process, leaving a depletion zone which is devoid of all mobile charge carriers. This zone forms the sensitive volume of the radiation detector. When a bias voltage is applied over the detector the depletion zone is increased.

3.3.2 Scintillation detectors

A scintillation detector consists of a scintillating material optically coupled to a photomultiplier (PM) tube. When hit by ionizing radiation, which causes excitations in the atoms and molecules in the material, a scintillating material emits flashes of light. When these scintillations hit the photocathode of the PM tube, they will cause a weak current of photoelectrons to be emitted. This current is then amplified by an electron multiplier system in the PM tube known as a dynode chain, and the amplified current will finally reach the anode of the PM tube, constituting the output signal from the scintillation detector.

3.3.3 Gaseous ionization detectors

A gas-filled ionization detector — an ionization chamber, a proportional chamber or a Geiger-Müller counter — is based on the principle of the collection of electron-ion pairs created in a gas by charged particles passing through it. The gas, usually a noble gas, e.g. argon, is enclosed in a cylindrical container with conducting walls, which function as the cathode of the detector. Along the axis of the cylinder, a conducting wire — the anode of the detector — is suspended. When a positive voltage, relative to the walls, is applied to the wire, a radial electric field is created. When ionizing radiation enters the cylinder, electron-ion pairs will be created, and the electric field will accelerate the electrons toward the anode and the positive ions toward the cathode.

3.4 Vacuum window

The most important feature of a vacuum window is that it must be able to withstand the pressure difference it will be subjected to — air pressure, 1013 mbar, on one side and vacuum, i.e. of the order of 10^{-6} mbar, on the other. Besides this property, a vacuum window should contribute as little as possible to additional spreading of the ion beam. Thus, the vacuum window must be manufactured from a material that can be made very thin and still be sufficiently strong. The most common vacuum window materials used in SIHFs for cell irradiation are Si_3N_4, a few hundred nm thick, and Mylar, a few μm thick. The area of the window is usually about 1 mm^2. In the table below, the vacuum windows used at some SIHFs for cell irradiation experiments, operational or under construction, are given. For comparison, the straggling of a 2.55 MeV proton beam caused by a 100 μm air gap is 0.39 μm.

SIHF	Window material	Window thickness	Beam straggling
CENBG, Bordeaux	Si_3N_4	150 nm [34]	13 Å
RARAF, New York	polypropylene	[35]	
GCI, Oxford	Mylar	3 μm [36]	36 nm
GSI, Darmstadt	Si_3N_4 with 20 nm Au and 50 $\mu g/cm^2$ CsI	200 nm [37]	11 Å
JAERI, Takasaki	microaperture on a tantalum disc	[46]	
Krakow	Si_3N_4	200 nm [39]	17 Å
LIPSION, Leipzig	Si_3N_4	100 nm [40]	4 Å
LNL-INFN, Legnaro	bi-aluminized Mylar	10 μm [41]	191 nm
Lund NMP	Si_3N_4	200 nm, [25]	10 Å
MIT, Boston	Mylar	1.4 μm [42]	36 nm
PTB, Braunschweig	Mylar	5 μm [43]	88 nm
SNAKE, Munich	Kapton	7.5 μm [47]	44 nm
Surrey, Guildford		[45]	

3.5 Cell culture dish

When using post-cell detection, an additional requirement on the experimental set-up is that the ions must retain sufficient energy, to penetrate the cell substrate on which the cells are cultured, in order to reach the detector. Due to this fact, standard plastic Petri dishes, normally used for cell culturing, may not be the best alternative. Most facilities performing single-cell irradiation experi-

ments have developed their own cell dishes, made to suit the specific conditions at the facility in question. The most common choice of cell substrate material is some kind of thin plastic foil — often Mylar or polypropylene. Another alternative is to grow cells on a thin Si_3N_4 wafer. In the table below, the cell dishes used at some SIHFs for cell irradiation experiments are given, along with information about the orientation of the cell dish.

Some of these cell substrate materials are inherently cell-friendly — meaning cells readily attach to and grow on the surface, without any prior treatment — while others are naturally cell-unfriendly and must be treated in such a way as to create a surface onto which cells can attach and grow. This treatment usually involves coating the substrate with a cell-friendly protein. This apparent disadvantage was turned into an advantage in the study described in Paper III, where a patterned cell dish was fabricated by partially covering a cell-unfriendly substrate with a cell-friendly protein, creating small isolated islands on which cells could grow.

SIHF	Cell dish material	Cell dish thickness	Dish orientation
CENBG, Bordeaux	polypropylene or Mylar	4 μm [34] 2 μm	Vertical
RARAF, New York	polypropylene	3.88 μm [35]	Horizontal
GCI, Oxford	polypropylene or Mylar	4 μm [36] 3 μm	Horizontal
GSI, Darmstadt	polypropylene	4 μm [37]	Vertical
JAERI, Takasaki	CR-39	100 μm [46]	Horizontal
Krakow	Si_3N_4	500 nm [39]	Vertical
LIPSION, Leipzig	Si_3N_4	200 nm [40]	Vertical
LNL-INFN, Legnaro	Mylar	7 μm [41]	Vertical
Lund NMP	SU-8	5 μm [25]	Vertical
MIT, Boston	polypropylene	4 μm [42]	Horizontal
PTB, Braunschweig	Teflon	1.5 - 25 μm [43]	Horizontal
SNAKE, Munich	Mylar	6 μm [47]	Vertical
Surrey, Guildford		[45]	Horizontal

Chapter 4

Biological effects of ionizing radiation

Ionizing radiation, i.e. radiation that is capable of ejecting orbital electrons from an atom and consequently producing chemical and biological changes, can be divided into two categories, as already discussed in Section 2.1, charged or neutral particles, and electromagnetic radiation. Charged particles are directly ionizing, while neutral particles and electromagnetic radiation are indirectly ionizing.

4.1 Definitions of dosimetric units

Linear energy transfer

The linear energy transfer, LET, is a quantity defining the amount of energy locally deposited per unit path length as a particle travels through a medium. Generally, LET is the same as dE/dx, the linear stopping power, if bremsstrahlung can be neglected. The unit of LET is keV/μm, and radiation is characterized as being either high-LET or low-LET. For any given type of charged particle, the LET, and thus the biological effect, will increase with decreasing particle energy. Alpha particles and heavy ions are considered to be high-LET particles, with an LET typically above 100 keV/μm, whereas protons, electrons and photons are low LET particles, with an LET of the order of 1 keV/μm [48].

Absorbed dose

The absorbed dose (D) is a measure of the total energy absorbed per unit mass, and the unit is the Gray, where 1 Gy = 1 J/kg. The absorbed dose does not take into account the dose rate or the type of radiation, although these two factors play an important role in determining the biological effects of the radiation.

Relative biological effectiveness

The biological damage resulting from irradiation will vary depending on radiation type and energy. The relative biological effectiveness (RBE) is defined as the ratio of a certain dose of radiation to the dose of 250 keV X-rays that would produce the same biological effect — this ratio varies between 1 and 20. However, RBE is not easy to measure in practice, and the concept of quality factor has been introduced instead.

RBE as a function of LET

For a given type of radiation, the relative biological effectiveness is a function of the linear energy transfer. In the case of alpha particles, the RBE increases with increasing LET, reaching a maximum for an LET of about 100 keV/μm; at higher LET values, the RBE decreases again. This is explained by the fact that at the ionization density of 100 keV/μm, the average distance between two ionizing events well matches the diameter of the DNA double helix, 2 nm. Thus, radiation with this ionization density has the highest probability of causing a DNA double strand break (see Section 4.2.2 for more details on DNA damage) by the passage of one single particle. A single particle track of more sparsely ionizing radiation, such as an X-ray, has a low probability of causing a double strand break, i.e. usually more than one particle track is needed. In the case of more densely ionizing radiation, the double strand breaks are indeed produced, but the extra energy imparted by additional ionization does not cause more biological damage, since the double strand break has already been caused [49]. For protons, the maximum RBE is at an LET value of around 20 keV/μm [50].

Quality factor or Radiation weighting factor

The quality factor or radiation weighting factor, w_R, takes into account the fact that the density of ionization, that is, the distribution of ionizing events along the track of the particle, varies depending on the type of particle. The more densely ionizing the radiation, the more local damage it will cause to the biological sample. Radiation is classified as sparsely or densely ionizing. For any given type of particle, the ionization density decreases with increasing particle energy. Alpha particles lose all of their energy over a very short path length, as

opposed to electrons and photons, which will distribute their energy loss over a much longer path, so that only a relatively small amount of energy is lost in any given segment of the path. Due to their much larger energy deposition over a short interval, alpha particles are said to be more densely ionizing than electrons and photons, and consequently a certain dose of alpha particles will have a greater probability of cell damage than the same dose of, for example, γ-rays. The radiation weighting factor ranges between 1 and 20, see the table below [10, 48]:

Radiation type	w_R
X-rays	1
γ-rays	1
Electrons	1
Neutrons, dep. on energy	5-20
Protons, keV energy	2-5
Protons, MeV energy	5-10
Alpha particles	20
Heavy ions	20

Equivalent dose

The equivalent dose, H_T, is a normalized measure of the biological effect of radiation on the organ/tissue, based on dose and ionization density, and the unit is the Sievert, where 1 Sv = 1 J/kg. Equivalent Dose = Absorbed dose $\times$ Radiation Weighting Factor

Effective dose

Depending on which tissue/organ has been exposed to radiation, the probability of developing cancer or other biological effects will vary. This can be described using the concept of effective dose (E) and the tissue weighting factor, w_T, which is defined for different organs, depending of their radiosensitivity. The organ weighting factor accounts for: (1) the probability of developing lethal cancer, (2) the probability of developing non-lethal cancer, (3) the probability of hereditary effects, and (4) the relative shortening of lifetime due to radiation exposure. The effective dose is calculated as the sum of the tissue weighting factor $\times$ the equivalent dose, over the different organs/tissues that have been exposed. The unit of the effective dose is the Sievert.

4.2 Mechanisms of damage

4.2.1 Direct vs. indirect action of radiation

Given that the critical target in a biological sample, e.g. a cell, is the DNA, damage to the DNA is the main reason for the production of different biological effects.

Direct action

In case of high-LET radiation, e.g. alpha particles, the dominant mechanism is the direct ionization or excitation of atoms or critical targets in a cell, leading to breakages of the chemical bonds of the DNA. If RH is a complex hydrogen-containing biological molecule, direct ionization can take place as follows [48]:

$$RH \rightarrow RH^{+} + e^{-} \tag{4.1}$$

Ionization is followed by dissociation of the ion:

$$RH^{+} \rightarrow R\cdot + H^{+} \tag{4.2}$$

where $R\cdot$ is a free radical. A free radical is an electrically neutral atom or molecule with an unpaired orbital electron in an outer shell, and thus possesses a high degree of chemical reactivity. If it is part of a biological system such as a chromosome, the $R\cdot$ radical can cause alterations — lethal as well as non-lethal — to the biological system. A non-lethal alteration can lead to genetic mutation.

Indirect action

In the indirect case, the radiation interacts with other atoms or molecules in a cell, especially H_2O, to produce free radicals, which in turn can reach and damage critical targets in the cell, resulting in indirect ionization of the DNA of the cell. Indirect ionization typically follows the following steps [48]. First, the water is ionized by the radiation:

$$H_2O \rightarrow H_2O^{+} + e^{-} \tag{4.3}$$

where H_2O^{+} is an ion radical.The free electron can then react with a neutral water molecule, forming

$$H_2O + e^{-} \rightarrow H_2O^{-} \tag{4.4}$$

Both the negative and the positive ion radicals are unstable and can dissociate:

$$H_2O^+ \rightarrow H^+ + OH\cdot \tag{4.5}$$

$$H_2O^- \rightarrow H\cdot + OH^- \tag{4.6}$$

Alternatively, the ion radical can react with water [1]:

$$H_2O^+ + H_2O \rightarrow H_3O^+ + OH\cdot \tag{4.7}$$

where $OH\cdot$ is the highly reactive hydroxyl radical and $H\cdot$ is the hydrogen radical. This radical has 9 electrons, meaning that one electron is unpaired. In an environment of organic matter, such as a cell, these free radicals can combine with the biological molecule RH to produce the free radical $R\cdot$:

$$OH\cdot + RH \rightarrow R\cdot + H_2O \tag{4.8}$$

$$H\cdot + RH \rightarrow R\cdot + H_2 \tag{4.9}$$

4.2.2 DNA damage and DNA strand breaks

The double-helix structure of DNA (deoxyribonucleic acid) consists of two strands, connected by hydrogen bonds between the bases. The backbone of DNA, making up each strand, consists of sugar and phosphate groups, and attached to the backbone are the bases. There are four different bases, thymine, cytosine, adenine and guanine, and the sequencing of these bases on the strands specifies the genetic code. Adenine must pair with thymine, and guanine must pair with cytosine. When a cell is irradiated by ionizing radiation, the DNA molecule can suffer different types of damage, commonly single- or double-strand breaks. An energy of a few tens of electron volts is enough to break the DNA helix [51]. Figure 4.1 shows an illustration of different DNA strand breaks caused by radiation.

Thanks to the well-defined, repetitive nature of the DNA molecule, a single strand break (SSB) can often be repaired without difficulty, using the opposite strand as a template. This is also true for breaks in both strands, if the two

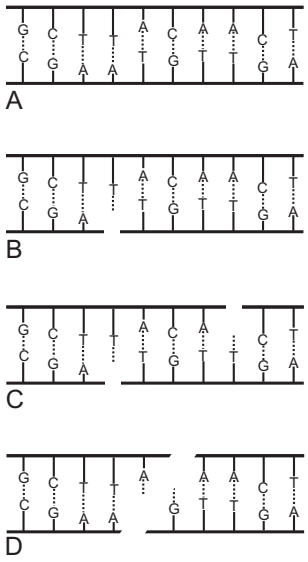

Figure 4.1: A: A two-dimensional representation of the normal DNA double helix. B: A DNA single strand break, C: Two DNA single strand breaks in opposite strands — as they are well-separated, they can be repaired independently, using the opposite strand as a template, D: A DNA double strand break, that is two DNA strand breaks in opposite strands, where the breaks are separated by only very few base pairs — the DNA double helix will break in two pieces.

breaks are well separated, as they can in this case be treated and repaired as separate breaks. Misrepair may, however, lead to a mutation. DNA double-strand breaks (DSBs), on the other hand, are the basis of most biological effects [49]. If the breaks in both strands are located opposite one another or separated by no more than a few base pairs, this will cause a DSB. DNA DSBs may lead to cell death, mutation or carcinogenesis. The ratio of DSBs to SSBs in irradiated cells is about 0.04 [1], and the number of DSBs increases linearly with dose.

4.2.3 Mechanisms of cell killing

The cell nucleus is considered to be more radiosensitive than the cytoplasm of the cell, meaning that the nucleus, rather than the cytoplasm, is considered to be the main target for radiation-induced cell lethality. The chromosomal DNA is thus the main target for cell killing, however, the nuclear membrane may

also be involved [1].

Apoptosis

Apoptosis, programmed cell death, from the Greek, meaning dropping off or falling (like petals from a flower), occurs in normal tissue, and can be induced by radiation in normal tissue and in some tumours. Apoptosis is a highly cell-type dependent cell killing mechanism. When a cell is committed to die, it will first cease to communicate with its neighbours. The dying cell then rounds up and detaches from its neighbours. The cell then shrinks and separates into a number of fragments, or apoptotic bodies, some containing cytoplasm only and some also containing nuclear fragments [1].

Mitotic death

Mitotic death is the most common form of cell death resulting from radiation — the cell dies as it is attempting to divide, because of damage to its chromosomes. Death can occur either in the first division or in a subsequent division of the cell. A close quantitative relationship has been established between cell killing and the induction of specific chromosomal aberrations [1].

4.3 Non-DNA-targeted effects

Although the standard model for the biological effects of ionizing radiation has been based on the assumption that nuclear penetration and subsequent directly induced DNA damage is necessary to trigger damage to a biological cell, it has in recent years been shown that neither nuclear hits nor cell hits are in fact required [52, 53]. Cells, whose nuclei and DNA have not been directly irradiated and damaged by ionizing radiation, have been found to express a number of biological effects similar to those expressed by cells in which the DNA has been targeted by ionizing radiation. These are known as non-DNA-targeted effects, and are particularly pronounced at low radiation doses [54]. In this thesis, one of the non-DNA-targeted effects of ionizing radiation was studied — the bystander effect. Other non-DNA-targeted effects are discussed briefly below for completeness.

4.3.1 Bystander effects

Cells that were not themselves irradiated, but were growing in the vicinity of directly targeted cells or were cultured in cell medium harvested from irradiated cells, have been found to exhibit responses similar to the ones of the directly exposed cells [1]. Two possible pathways whereby these bystander signals can be transmitted have been pinpointed — the medium-mediated pathway, where

soluble factors, such as free radicals, reactive oxygen species (ROS), nitric oxide and cytokines, are transferred between cells via the cell culture medium, and the direct cell-to-cell contact pathway, where cells use gap junction intercellular communication (GJIC) to communicate with their neighbours [55]. Several different bystander responses have been described, including apoptosis, sister chromatid exchange (SCE, chromosomal rearrangement), micronuclei formation, genomic instability, gene mutations [56, 57]. The above mentioned responses cause cell damage. However, some possibly non-damaging bystander effects have also been found, e.g. adaptive responses (that are radio-protective) as well as increased cell proliferation [57]. The medium-mediated pathway and the GJIC-mediated pathway are not independent or mutually exclusive, but co-exist and are related in some way. However, GJIC may play a dominant role in heavy-ion- induced bystander effects [58].

Soluble factors

As the focus of the studies described in this thesis work was on medium-mediated bystander effects — results are presented in Paper IV and chapter 6.3 — rather than GJIC-mediated effects, this pathway will be described in more detail in this section. Nitric oxide, NO, has been found to be excreted from irradiated cells and transmitted to non-irradiated neighbouring cells, triggering several different effects in the bystander cells. Co-culture studies in which carbon-ion-irradiated human salivary gland (HSG) cells were cultured with unirradiated HSG cells have shown an increase in cell proliferation and micronucleus induction in the unirradiated cells [59]. Treatment with an NO scavenger eliminated these effects. In a similar set-up, co-culturing unirradiated lymphoma cells with HSG cells irradiated either with high-LET carbon ions or low-LET X-rays revealed that apoptosis and necrosis were induced in the unirradiated cell culture, but that these effects could be reduced to the control level by treating the cells with an NO scavenger [60]. In both experiments, the concentration of nitrite in the co-culture medium was found to correspond well to the cell proliferation and micronucleus formation in the unirradiated cells, as well as to the decrease in the viability of the irradiated HSG cells. It was also shown that the production of nitrite depends on the LET and the dose to the HSG cells.

Another study has revealed that NO secreted from X-ray-irradiated cells reduces cellular radiosensitivity. In that study [61], two human glioblastoma cell lines were used — either in co-cultivation experiments or in experiments where the cells were cultured in medium from irradiated cells. The results showed that the accumulation of inducible NO synthase caused by the X-ray irradiation could be abolished either by the addition of an inhibitor for inducible NO synthase (co-cultivation experiments) or by the addition of an NO scavenger (medium-transfer experiments). Cells cultured in medium from irradiated cells

were less radiosensitive than cells cultured in fresh medium.

Different reactive oxygen species, ROS, that can influence the environment in and around human cells are superoxide anions O_2^-, hydrogen peroxide H_2O_2, hydroxyl radicals $OH\cdot$ and oxides of nitrogen [52]. ROS are known to be important in normal cell functioning, including cell signalling pathways, but too high levels of ROS can lead to DNA damage, resulting for example in aging, apoptosis and even cancer. An investigation of the role of superoxide in causing sister chromatid exchanges (SCEs) in bystander cells [62] revealed that culture medium transferred from human lung fibroblasts exposed to alpha particle irradiation induced excessive SCEs in unirradiated fibroblasts. The SCE levels in these cells were similar to those in cells that had actually been exposed to alpha irradiation. It was also found that irradiated culture medium alone could induce SCEs in unirradiated cells, if the medium was irradiated immediately prior to being added to the cells. If the irradiated medium or the medium from the irradiated cells was treated with the superoxide dismutase SOD just prior to being added to the unirradiated cells, the SCEs in the cells were reduced to a level comparable to the control cells. SOD functions as an antioxidant in that it catalyses the conversion of superoxide anions into oxygen and hydrogen peroxide [62].

In a similar investigation, the cellular production of superoxide and hydrogen peroxide following alpha irradiation was assessed directly, using flow cytometry [63]. Normal human lung fibroblasts were irradiated with alpha particles and, compared with sham irradiated fibroblasts, increases in O_2^- as well as in H_2O_2 production were observed, not only in the irradiated cells but also in unirradiated cells cultured in the alpha-particle-exposed medium or in medium from alpha-irradiated cells. Also, more cells produced intracellular H_2O_2 than had received either a nuclear or a whole-cell hit by at least one alpha particle.

Gap junction intercellular communication

Gap junctions are intercellular membrane channels, about 2 nm in diameter, directly linking the cytoplasms of neighbouring cells. Via these channels small molecules can be directly transferred from the interior of one cell into that of a neighbouring cell [64]. Little is known about the signals that can be transferred via GJIC [51], but the protein connexin 43 (the connexin proteins form the gap junctions [2]) appears to be required [57].

In a study where confluent cell cultures were exposed to a low fluence of alpha particles, such that only about 1-2 % of the cell nuclei were actually traversed by an alpha particle, evidence for gap junction-mediated intercellular communication transmitting damage signals to nonirradiated cells was found [65]. Several different cell types were used in that study, including normal human fibroblasts, mouse embryo fibroblasts and rat liver epithelial cells —

some of the cell lines having been genetically manipulated so as to no longer be able to perform GJIC. The results showed that in cell cultures that had been made GJIC-deficient or where lindane (which inhibits gap junction intercellular communication by changing the permeability of the gap junction channels as well as the number of gap junctions) had been added, changes in gene expression and micronuclei formation in bystander cells could be prevented. Only in GJIC-competent cell cultures could these studied end points be detected in bystander cells.

In another study [64], Chinese hamster lung fibroblasts (V79 cells) were radiolabelled with a β particle emitter and then co-cultured with unlabelled V79 cells — 100 %, 50 % or 10 % of the cells in the cell culture were labelled. The surviving fraction of cells was studied as a function of the activity of the labelled cells, with and without the free radical scavenger DMSO and/or the GJIC inhibitor lindane; the presence of GJIC was assessed using flow cytometry. In that study, lindane proved to be more efficient in protecting the unlabelled cells than DMSO, however, the most protective effect was achieved when combining the two substances.

4.3.2 Other non-DNA-targeted effects

Besides the bystander effect, a number of other non-DNA-targeted effects have been identified [53]. One such effect is the adaptive response, where cells that have received a low priming dose, prior to being exposed to a higher dose show less response to the higher dose, in terms of survival, mutation and chromosomal damage. Another effect is low-dose hypersensitivity, where cells have been observed to show an increased sensitivity (hypersensitivity) to radiation at low doses, followed by a relatively radioresistant phase at higher doses.

At very low dose rates, effects such as levels of mutation or transformation that follow an inverse dose rate relationship, i.e. more pronounced effect with lower dose rates, have been found. This is known as the inverse dose-rate effect. Genomic instability indicates changes, such as chromosomal changes, mutation and cell death, that have been found in the surviving offspring of irradiated cells. Another effect is gene expression, meaning up- or down-regulation of genes, not being induced by direct DNA damage, shown in low-dose studies.

4.4 Biological markers for cell damage

Fluorescence microscopy stains

In the experiments described in Chapter 6 Hoechst 33342 stain was used as a general stain, staining all cells in the cell cultures. Hoechst binds to DNA and is able to cross intact cell membranes [66]. The stained cells were examined

using fluorescence microscopy, where cells containing Hoechst stain will emit blue light.

Propidium Iodide stain (PI) was used to identify the dead cells in the cell cultures. PI binds to DNA (and also to RNA), but is membrane-impermeant, which means that it cannot pass through the membrane of viable cells [67]. Only dying or dead cells have a permeable membrane, allowing substances to leak into as well as out of the cell. Cells containing PI will emit red light when inspected in a fluorescence microscope.

Chapter 5

Search for a pre-cell detector

Of the single-hit detectors currently in use at SIHFs to detect the ions before they encounter the cells in the culture, one is widespread, namely a thin (5 to 50 μm) plastic scintillator coupled to a photomultiplier tube. The first part of this thesis is concerned with investigating a possible alternative to the scintillator + PMT detection method — namely an ultra-thin semiconductor transmission detector made of silicon. As has already been mentioned in Section 3.3, the pre-cell hit detection method provides the opportunity of irradiating cells in a hydrated atmosphere, where an arbitrary amount of cell medium is allowed. This method would furthermore be particularly advantageous when moving away from irradiating cell monolayers and instead experimenting on thicker cell layers, tissues or even semi-thick organisms, of thicknesses similar to that of the tardigrades.

An additional feature, and possibly an improvement in the detection system, would be the possibility of using the pre-cell detector not only as single-hit detector, but also as a vacuum window simultaneous. This would reduce the amount of material the ion beam has to pass through before reaching the cell culture; thus reducing the scattering of the ion beam. This thesis presents studies on two different thin Si transmission detectors, to assess their suitability as combined vacuum windows and pre-cell hit detectors for use in single-cell irradiation experiments. The experiments described were carried out at the Lund NMP.

5.1 The detectors

Thin silicon detectors, originally intended to be used in ΔE-E detector telescopes [68], were tested as pre-cell detectors. The two detector types differed in thickness and area, as well as design bias. The first specially designed trans-

mission detector had an area of 4 mm^2, a thickness of 9 μm and a design bias of only 2 V. The experiments performed on this detector are presented in Paper I. The second, improved, detector type had an area of 1 mm^2, a thickness of 8-10 μm and a design bias of -7 V. The experimental results from these detectors are presented in Paper II.

The 9 μm detector was mounted on a frame, which in turn was mounted on the sample wheel in the micro-beam line target chamber. The 8-10 μm detectors, which were investigated at the nano-beam line, were mounted on a much smaller frame which was mounted vacuum tight on one end of a small cylinder. The cylinder is of the same type that is normally used at the Lund NMP as vacuum-tight end cap on the beam extension pipe utilized in external beam experiments (in that case the cylinder is sealed with a Si_3N_4 window). Thus, the ability of the detector to function as vacuum window could also be investigated. The cylinder also fits in the sample holder in the nano-beam line target chamber.

5.2 Characteristics investigated

The first task was to evaluate the signal-to-noise ratio of the 9 μm detector, or rather how well the signal was differentiated from effects such as incomplete charge collection and edge effects, as well as noise. Incomplete charge collection, i.e. charge carrier loss due to e.g. trapping of holes, will manifest itself as a shift in the peak in the transmission detector spectrum towards lower energies, as the output signal is proportional to the charge collected [69]. Edge effects are the result of ions having penetrated the transmission detector at the edge of the active area, where the detector is thicker, and will cause the peak to shift towards higher energies. Once it had been established that the detector did indeed give a clear, well-defined signal, the next task was to evaluate the efficiency of the detector, and whether it varied with the bias applied. Based on the results obtained from the experiments on the 9 μm detector, it was concluded that further investigations should be carried out, if possible, on an even thinner detector.

As the bias had proved to influence the efficiency, a number of different bias voltages were investigated on the new 8-10 μm thick detectors. However, attention was shifted from the dependence on the applied bias alone to include that on the particle energy and type. Initially, an alpha particle emitter was used to study the efficiency, and later protons from the Lund NMP were utilized, with very promising results.

5.3 Experimental approach

To assess the efficiency of the detectors, a ΔE-E "telescope" was constructed, using the thin transmission detector as the ΔE part and a Hamamatsu windowless p-i-n diode as the E part. The "telescope" was bombarded by alpha particles (and later protons), and the number of alpha particles detected in the thin transmission detector was compared with the number of alpha particles detected in the p-i-n diode. Only ions that had passed through the centre of the transmission detector were counted, to ensure that the true performance of the detector was evaluated. These values were retrieved directly from the KMax software [70] energy spectra. The energy spectra were calibrated and compared with SRIM simulations. Figure 5.1 shows the possible fates of ions encountering the transmission detector, and the corresponding energy spectra, including ions transmitted through the centre and the edge of the detector as well as stopped ions.

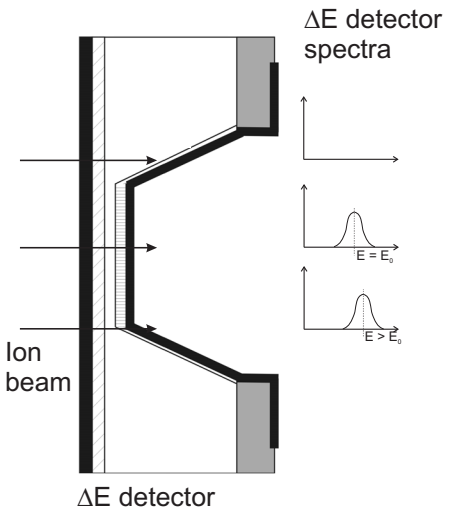

Figure 5.1: ΔE detector spectra resulting from stopped ions (top), ions transmitted through the centre (middle) and the edge (bottom) of the ΔE detector.

All experiments were carried out in STIM imaging mode, with a beam current of the order of 1000 protons/s. Initially, as is reported in Paper I, only 2.55 MeV protons were used, but in later experiments, as reported in Paper II, 2.55 MeV, 2.2 MeV and 2 MeV protons as well as alpha particles (5-9 MeV) were used.

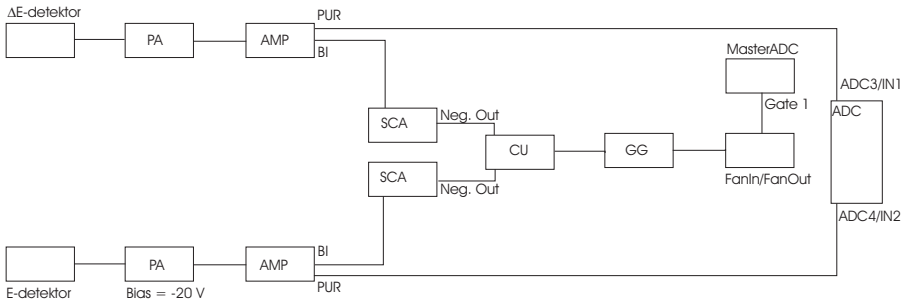

Figure 5.2: Circuit diagram of the experiment. PA = preamplifier, AMP = amplifier, SCA = single channel analyser, CU = coincidence unit, GG = gate generator, ADC = analog-to-digital converter

Besides the direct comparison of the number of ions detected, the surface of the thin detector was also of interest. The proton beam was deliberately scanned outside the active area of the thin detector to map the transition between the detector window and the edge. To image the active area as well as the edges of the thin detector, maps were constructed using STIM imaging. Furthermore, 2D maps of the coincidences in the pulse height spectra of the E detector and the ΔE detector were used to investigate the origin of the detected pulses. Figure 5.2 shows a circuit diagram of the experimental set-up. Using the coincidence unit (CU), different triggering conditions could be set for data acquisition — triggering on the ΔE detector alone, on the E detector alone, or on the two detectors together. For each gate that was generated, independent of the logics, data from the two detectors was collected. The use of the term "coincident" in Paper I is somewhat misleading and should be clarified at this point. Coincidence between the two signals was not required in the electronics set-up, however, because of the low beam current, in a "true" event, the same proton has to be registered in both detectors. This means that for every event in the E detector a corresponding event should appear in the ΔE detector, and that all pairs of events should have the same energy. A more appropriate term in this case would be "simultaneous".

5.4 Evaluation of the data

Figures 5.3 and 5.4 show, complementary to data presented in Paper I, an energy spectrum from the 9 μm ΔE detector and the E detector spectrum, respectively, at a proton energy of 2.55 MeV. As stated in Paper I, a complete efficiency was not obtained. At best, a value of 76 % was achieved, but at a

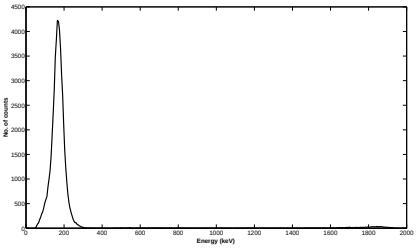

Figure 5.3: Energy spectrum of the ΔE detector, 2.55 MeV protons.

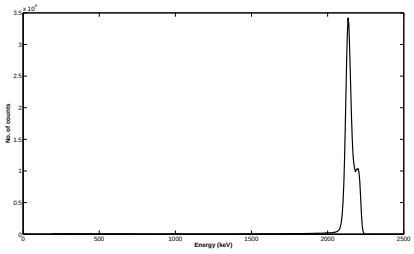

Figure 5.4: Energy spectrum of the E detector, 2.55 MeV protons.

far higher bias voltage, 20 V, than the design bias of 2 V.

The next "generation" of 8-10 μm detectors (area = 1 mm^2) were first investigated using the alpha emitter Th-228. When comparing the number of detected ions in the two detectors, the result was close to perfect match; the efficiency never falling below 99 %, which was very encouraging.

After the initial alpha source experiments, the proton beam at the Lund NMP was used, and three different energies were chosen: 2.55, 2.2 and 2 MeV. During these experiments, the bias on the thin detector was also varied, to monitor any possible effect on the efficiency. Three different bias voltages were chosen, -6 V, -15 V, -20 V, however, no significant difference in the efficiency was seen. The efficiency for 2.55 MeV protons was 70 %, for 2.2 MeV protons 85 % and finally, for 2 MeV protons the desired 99 %.

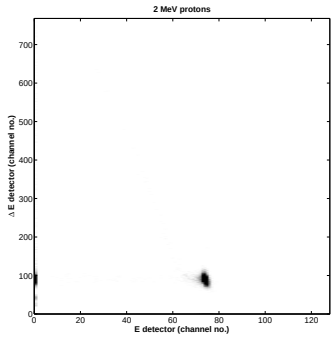

Figure 5.5: E-ΔE plot, 2 MeV protons — no energy tail present.

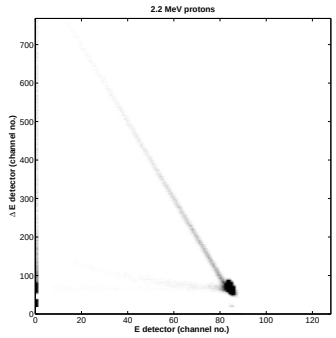

Figure 5.6: E-ΔE plot, 2.2 MeV protons.

In addition to the efficiency measurements, the active area of the detector

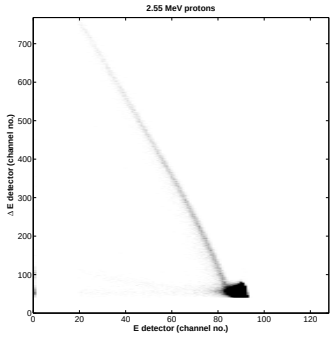

Figure 5.7: E-ΔE plot, 2.55 MeV protons.

was characterized in greater detail. A description of similar work studying detector features can be found in [71]. In Figures 5.5-5.7, the results of scanning only inside, compared to scanning inside as well as outside, the active area of the detector can be seen. Scanning outside the active area resulted in a tail corresponding to the increased energy loss at the edge of the detector. This phenomenon is described in more detail in Paper II. In all cases, the sum of the energy loss in the ΔE detector and the energy loss in the E detector was practically constant (although not necessarily adding up to the full energy of the incoming proton).

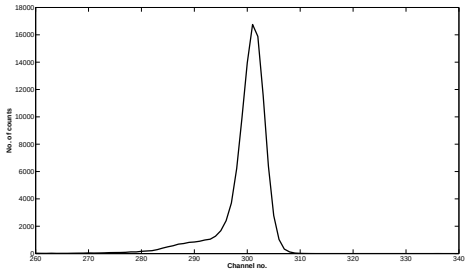

Figure 5.8: E detector energy spectrum, 2.55 MeV protons.

This behaviour can also be seen in the E detector energy spectra directly, as is demonstrated in Figure 5.8, where two regions can be identified: the peak and the low-energy tail. When these two regions are 2D mapped separately, see Figures 5.9 and 5.10, they reveal protons that have passed straight through

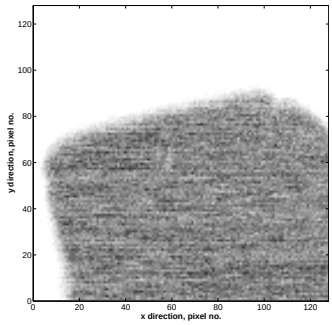

Figure 5.9: 2D image of the peak, channel numbers 294-308.

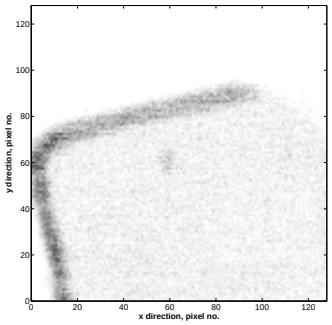

Figure 5.10: 2D image of the tail, channel numbers 270-294.

the middle of the ΔE detector and those close to the edge, thus losing more energy. Figures 5.9 and 5.10 are shown to illustrate or in another way explain the methodology of the experiments. First, they illustrate that the thickness of ΔE detector does appear to be even and, perhaps more importantly, that additional energy loss is only found along the edge of the detector. Second, they are an illustration of how the efficiency calculation was carried out — events with a lower energy in the E detector, that correspond to ions encountering the ΔE detector edge, were excluded from the efficiency calculation.

5.5 Outlook

The concept of a thin silicon transmission detector acting as vacuum window and pre-cell hit detector simultaneously is an appealing thought, and it does in fact, at least to a certain extent, appear to be realistic. However, a number of problems and concerns remain to be solved. The fact that the construction of the detector is quite fragile (i.e. very thin) cannot be circumvented, and the detector must instead be handled with care. The mounting of the detector, which in its present form is also fragile and constitutes an obstacle when working with the detector can, on the other hand, be improved. The repeated breakage of the connections can be avoided by mounting the detector differently. Changes must also be made to the mounting to minimize the air gap between the detector/vacuum window and the bottom of the cell dish.

In addition, the issue of break down of the detector — this problem was discussed in more detail in Paper II — should be solved, or at least investigated in more detail, to pinpoint the cause of break down, and what determines whether the detector will recover or not. This problem, that also may affect

the detector's suitability for routine use, is hypothezised to be a heating effect, and is observed after several hours of non-stop use. This could be the result of irradiation of the oxide, which has been shown to lead to an increased leakage current. The fact that the detector for no apparent reason stops working, and then appears to recover when it has been allowed to rest without any applied voltage for a period of time, could then correspond to the recovery of the oxide-silicon interface.

It also remains to be determined whether or not the detector functions properly when used simultaneously as a detector and vacuum window. This is, however, not an absolute requirement, as a separate vacuum window can be used instead. Studies must also be carried out to determine whether the advantage of reduced beam spreading when not using a separate vacuum window outweighs the risk of breaking the detector when a separate vacuum window is not used.

Chapter 6

Development of patterned cell substrates

The reason for developing a patterned cell dish, in which the cells grow in several isolated regions, was to study possible medium-mediated bystander effects of ionizing irradiation. The idea is to culture cells in several isolated islands in a cell dish, irradiate one of the cell islands on which a limited number of cells are growing, and study how the cells growing on the neighbouring, non-irradiated, cell islands respond. As the cells cannot communicate directly by cell-to-cell contact — due to the fact that they are physically separated — any effects seen in the neighbour cells must be the result of factors mediated across the cell dish via the cell culture medium. In this way, it is possible to rule out the influence of a gap-junction-mediated bystander effect. Another very interesting application is to use patterned cell dishes to grow different types of cells, e.g. cancer cells and healthy cells, in the same dish, while keeping the different cell types physically separated. Using this approach, it has been shown [72] that irradiating one type of cell in one region in the dish induces DNA damage in the other, non-irradiated cell type in a different region. In this study, normal fibroblasts and malignant glioma cells were irradiated with He-3 particles, and the endpoints studied were induction of micronuclei and the production of NO and ROS.

6.1 Fabrication of patterns

The patterned cell substrates were manufactured using the droplet microdispenser (modified inkjet spray technique) at the Department of Electrical Measurements and Industrial Electrical Engineering and Automation, Lund Institute of Technology, Lund University, and is described in Paper III. The choice

of cell substrate and coating was based on a literature survey that is described in more detail in Paper III. An 8 μm thick polypropylene film [73] was chosen as substrate and the mussel protein Cell-Tak [74] was chosen as coating. Rectangular acrylic glass aerosol filter holders were used as frames for the polypropylene foil as they fit the sample holder in the target chamber. Due to their rectangular shape they can easily be positioned and repositioned in the sample holder. Figure 6.1 shows the result of an attempt to culture cells on an untreated polypropylene foil.

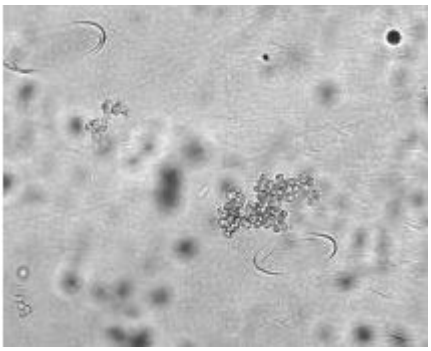

Figure 6.1: Cells cultured on a polypropylene foil, without any Cell-Tak treatment. Only floating, dead cells are present.

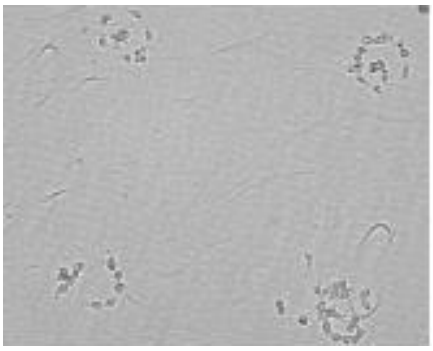

Figure 6.2: Spots spaced 500 μm apart, 2 droplets per spot.

The recommended concentration of Cell-Tak for coating a surface given by the manufacturer is 3.5 $\mu g/cm^2$ [75]. In the present experiments two different concentrations of the protein solution were used: 1.36 mg/ml and 2.4 mg/ml.

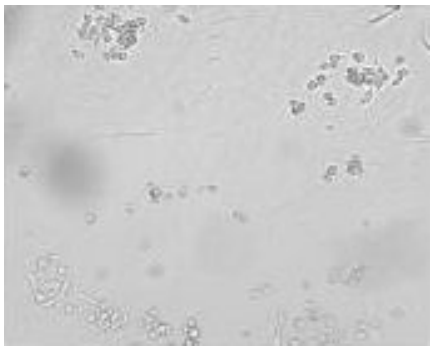

Figure 6.3: Spots spaced 500 μm apart, 3 droplets per spot.

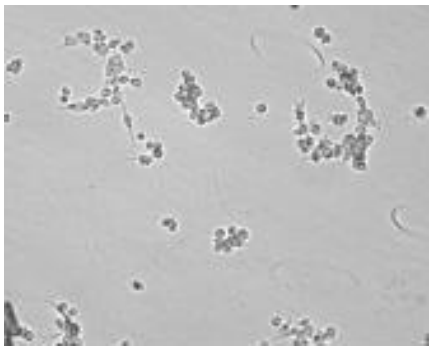

Figure 6.4: Spots spaced 500 μm apart, 5 droplets per spot.

With a droplet volume of 90 pl and a spot size on the substrate of about 100-150 μm, this corresponds to a total of about 2 droplets per spot. This corresponds roughly to the threshold amount required for cell growth on the substrate, see Figure 6.2. Figures 6.3 and 6.4 show a comparison between cell growth on three and five droplets per spot of the less concentrated protein, respectively. From these images it can be seen that when the protein coating is very thin, it tends to dry as a circle of protein, with no protein in the middle — a phenomenon known as a coffee stain — and that the cells grow accordingly. To achieve homogeneous cell growth, about ten droplets per spot are required, in the case of the more concentrated protein — see Figure 6.5. This figure depicts the ideal situation, with round spots in a well-defined, periodic matrix pattern without unwanted satellite droplets. The cells tend to grow somewhat differently depending on how closely spaced the spots are on the substrate.

If the spots are spaced close enough together, they will start to bleed into each other to a certain extent. Figures 6.5 and 6.6 show images of spots with a spacing of 200 μm and 150 μm, respectively, for comparison. A less than perfect example is shown in Figure 6.7, in which most of the spots are accompanied by a satellite droplet. Figure 6.8 shows how the cells grow when ten droplets of protein are used per spot (this photograph was taken in the same cell dish as that shown in Figure 6.5). No apparent improvement in cell growth was found when the amount of protein was increased to twelve droplets per spot.

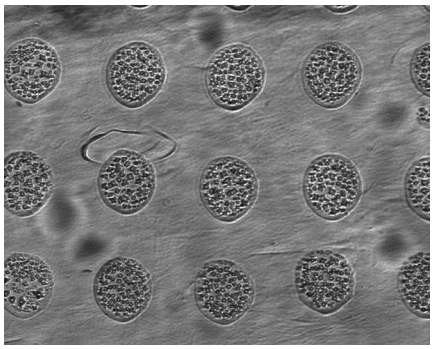

Figure 6.5: Spots spaced 200 μm apart.

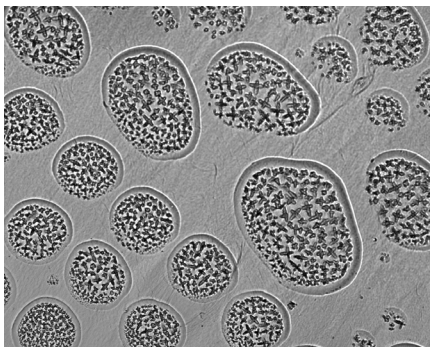

Figure 6.6: Spots spaced 150 μm apart.

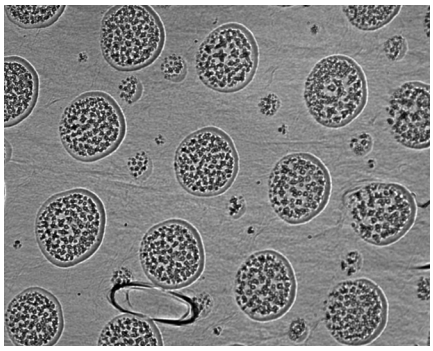

Figure 6.7: Spots spaced 200 μm apart, with satellites.

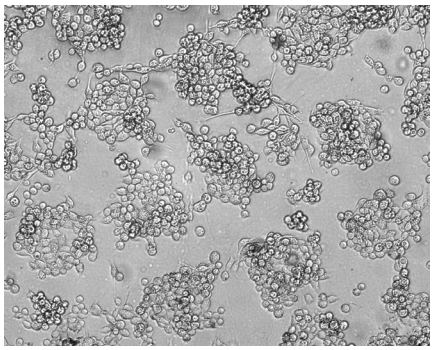

Figure 6.8: Cells cultured on a polypropylene foil, with ten Cell-Tak droplets per spot. Cells grow on the treated surface only.

6.1.1 Elemental analysis of patterns

As the elemental content of the mussel protein was not well-known, PIXE analysis of a few protein-coated cell substrates was carried out. The data was analysed using the GeoPIXE software [76]. This revealed that mainly sulphur, chlorine and zinc were present in the protein. In Figures 6.9 and 6.10 some results of the PIXE analysis, complementary to results shown in Paper III, are shown. Figure 6.9 shows a series of elemental maps, showing S, Cl and Zn. In Figure 6.10 a vertical section across a chlorine map of a larger coated area is shown to illustrate the evenness of the coating when it is dispensed over a larger surface.

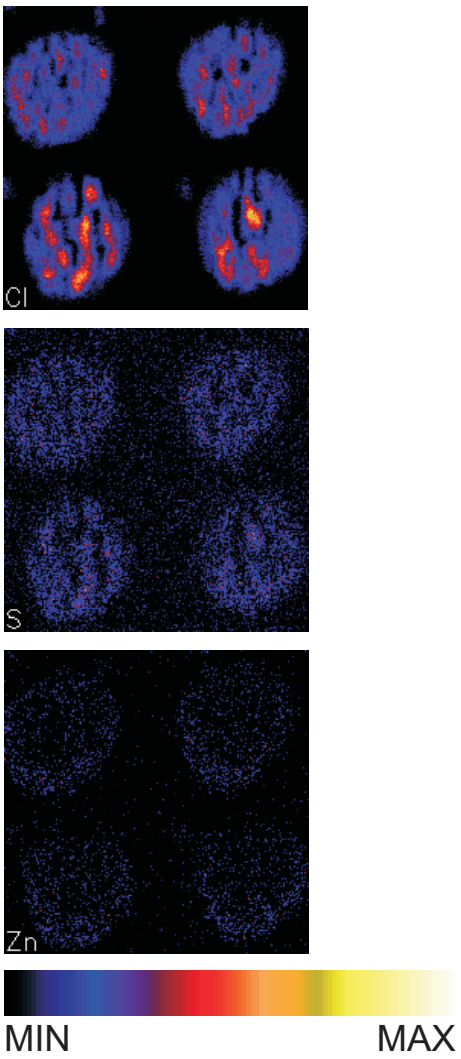

Figure 6.9: PIXE maps of the main constituents of the mussel protein Cell-Tak — chlorine, sulphur and zinc. The size of each map is 384 μm $\times$ 384 μm.

6.2 Biological experiments

All biological irradiation experiments performed so far have been conducted on the HepG2 cell line. HepG2 cells are human liver cancer cells, or hepatoma

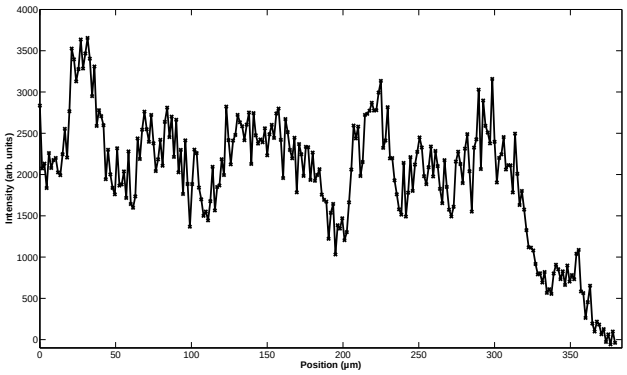

Figure 6.10: Illustration of the evenness of the protein coating when using the microdispensing technique to coat a larger surface.

cells, retrieved from an adolescent male suffering from hepatocellular carcinoma [77].

6.2.1 Biological endpoints

The aim of the experiments was to investigate cell death following exposure to ionizing radiation — in directly irradiated cells as well as in neighbouring, non-irradiated cells growing at some distance from the irradiated spot. The fraction of dead cells was calculated by comparing the number of cells that were stained with Hoechst with the number of cells stained with PI. (For details of the stains, see Section 4.5.) Cells were cultured up to 72 hours after irradiation, and dishes were inspected either 0, 24, 48 or 72 hours after irradiation, at which point PI was added to the dish in question. The results presented in paper IV are mean values from triplicate experiments. The hypothesis that the protein α_1-microglobulin could serve as a cell-protection agent, possibly by counteracting oxidative effects induced by the radiation, was tested. Furthermore, it was hoped that initial investigations using the patterned cell substrates would give an indication of, or confirm, whether or not cell death following irradiation could be attributed solely to GJIC-induced bystander effects.

α_1-microglobulin (α_1m) is a plasma and tissue protein, mainly synthesized in the liver, which has been identified in, for example, mammals. α_1m is involved in the defence against pathological oxidation caused by, for example, reactive oxygen species — ROS induce an increased expression of α_1m in liver and blood cell-lines. It has recently been indicated that α_1m has antioxidant

and cell-protective properties [78].

6.2.2 Irradiation protocol

The irradiation experiments carried out so far have been performed using an alpha source and not the proton microbeam at the Lund NMP. The reason for this is that the SIHF in Lund is still not fully operational — the cell recognition programme has not yet been implemented online. This means that non-targeted cell irradiation with a specific number of protons is possible, but it is not possible to determine exactly where the single protons have hit the cell sample. Thus, it is difficult to judge whether any fluorescence that appears after the irradiation is due to a direct proton hit or is not really "correlated" to the protons. When using the collimated alpha source — the set-up is described below — the area that has been irradiated can be identified with sufficient precision, as the bystander effects are studied several millimetres or even centimetres away from the irradiation spot, i.e. a distance far greater than the size of the collimator. However, it cannot be precisely determined which cells have been irradiated, neither can the exact dose to an individual cell be calculated.

In addition, it is not yet possible to irradiate the same amount of cells at the Lund NMP as can be irradiated using an alpha particle source. At some of the operational SIHFs, the cell throughput can be as high as 10,000 individually irradiated cells per hour [79]. With such high cell throughput, effects such as mutagenic and oncogenic endpoints can be studied. A cell throughput of $<$1000 cells per hour is sufficient for studies of, for example, apoptosis and cell death [80]. With the alpha emitter, many more experiments — although not with individually irradiated cells — can be carried out much faster, at much lower cost and with much less effort. Thus, to obtain sufficient data to be able to draw preliminary conclusions, the alpha particle source was a practical starting point. To determine whether or not α_1-microglobulin has any cell-protecting effect, it was important to test this with a fast, albeit, coarser method.

Furthermore, there is presently no biological cell laboratory located in the direct vicinity of the microprobe laboratory. This means that, when carrying out irradiation experiments at the Lund NMP, the cells have to be taken from their protected environment in the cell laboratory at the Biomedical Center (a distance of a few hundred metres) and transported to the microprobe laboratory and back, which will introduce unwanted and unnecessary confounding variables into the experiment. When travelling back and forth between the two laboratories, the biological environment cannot be fully controlled, and factors such as changes in temperature and humidity can be potentially harmful to the cells. It may thus be difficult to deduce what has actually caused any detected cell death.

The alpha source used to irradiate the cell cultures was a ^{228}Th source. To restrict the irradiation to a small, well-defined area, a mask with an opening

of 600 μm diameter was manufactured. A 10 mm diameter hole was drilled in a plastic Petri dish and a 125 μm thick Mylar foil was glued over the hole. A small hole was made in the Mylar foil, using a hypodermic needle attached to a syringe. This resulted in a small radioactive source holder with a 600 μm opening for the alpha particles to pass through. The count rate of alpha particles from the ^{228}Th source passing through the hole in the mask was measured and found to be 220 particles per second. The area of the collimator hole was 0.28 mm^2 and, given that the area of a cell is 140 μm^2, the number of cells that can be irradiated through the collimator is 2000. Thus, a cell will on average receive 0.11 alpha particles per second.

The drawback of using a radioactive source instead of a microbeam is that one cannot with certainty determine the number of particles delivered to any particular cell in a culture. Instead one has to use the Poisson distribution to calculate the percentage of cells being irradiated by a certain number of particles, based on the mean number of particles per cell [10, 58].

The ^{228}Th decays by emitting alpha particles with six energies ranging from 5 MeV to 9 MeV. The table below gives the spectral distribution together with the relative intensities of the six peaks and the LET at the respective energies. Based on these values, a weighted mean LET was calculated, which was used in the dose calculations.

α energy (MeV)	LET (keV/μm)	Rel. intensity (%)
5.42	86.31	21
5.68	83.51	19
6.04	79.87	7
6.28	77.71	20
6.78	73.51	20
8.78	61.73	13

The absorbed dose per alpha particle was calculated using the following relationship:

$$dose[Gy = J/kg] = LET[eV/\mu m] \cdot 1.602 \cdot 10^{-19}[J/eV] \cdot \frac{targetthickness[\mu m]}{targetmass[kg]} \tag{6.1}$$

where the thickness of a cell was assumed to be 4 μm, the mass of a cell 5.6 $\times$ 10^{-4} μg and the area of a cell 140 μm^2. The weighted LET used was 77.9 keV/μm, which gives an absorbed dose per alpha particle of 0.09 Gy.

To assess more accurately how well restricted the alpha particles are by the hole in the mask and how many cells that in practice can be hit by alpha particles through the opening in the mask, the track-etch plastic CR-39 was used, to visualize the alpha particles reaching the cell dish. Images of the

Mylar collimator and the CR-39 after being irradiated by the ^{228}Th source for 20 seconds can be seen in Figure 6.11. Both images are taken with 10 $\times$ magnification, and in the CR-39, few alpha particle tracks are visible outside the region shown, i.e. few cells not located directly beneath the collimator would be hit by alpha particles.

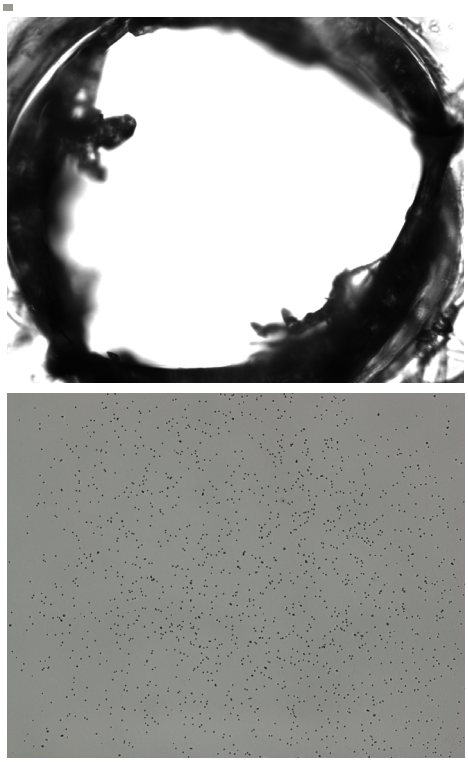

Figure 6.11: Photo (10 $\times$ magnification) of the hole in the Mylar collimator (above) and of alpha particle tracks in CR-39 (below). The diameter of the hole in the Mylar is 600 μm. The CR-39 was etched for 5 minutes in KOH (12 mol/l) at 80°C [34]. In the CR-39, only few tracks are visible outside the region shown in the photo.

6.3 Biological results

The biological results are mainly presented in Paper IV — some complementary data is given in this section. Three different irradiation times were used:

20 seconds, 1 minute and 3 minutes, which correspond to about 2, 6.5 and 20 particles/cell, and absorbed doses of 0.2, 0.6 and 1.8 Gy, respectively. According to the Poisson distribution, in the case of the 20-second irradiation, 82 % of the cells will receive a maximum of 3 particles and 62 % of the cells will receive a maximum of 2 particles. In the case of the 1-minute irradiation, 65 % of the cells will receive between 4 and 9 particles.

6.3.1 Cells in Petri dishes

All cells used in the experiments, irradiated as well as controls, were monitored for three days following the initial irradiation/sham irradiation. Images were taken once a day, using differential interference contrast microscopy (DIC) and fluorescence microscopy, starting immediately after the irradiation. Figures 6.12-6.15 are shown DIC images as well as fluorescence microscopy images of Hoechst- (blue) and PI- (red) stained cells, one day post-irradiation.

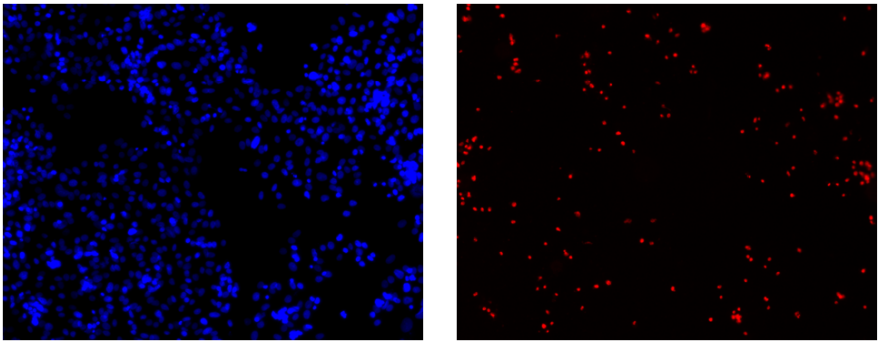

Figure 6.12: Control Petri dish, one day after sham irradiation. Hoechst stain to the left and PI stain to the right.

Both the irradiation spot itself and regions of the cell dish close to and far away from the irradiation spot were studied. By counting the percentage of dead cells in these images, it became evident that non-irradiated cells also suffered effects from irradiation, leading to increased cell death. As is discussed in more detail in Paper IV, it was evident that, compared to control cells (i.e. cells in dishes that were not irradiated), the alpha particle irradiation induced a time-dependent increase in cell death up to almost 75 % in the irradiation center and about 30 % in the peripheries of the cell dish. When comparing the three different doses, no dose-dependence was seen anywhere in the cell dish.

When α_1-microglobulin was added to the Petri dishes, the situation changed significantly, as can be seen in Figures 6.16-6.17. As is discussed in more detail

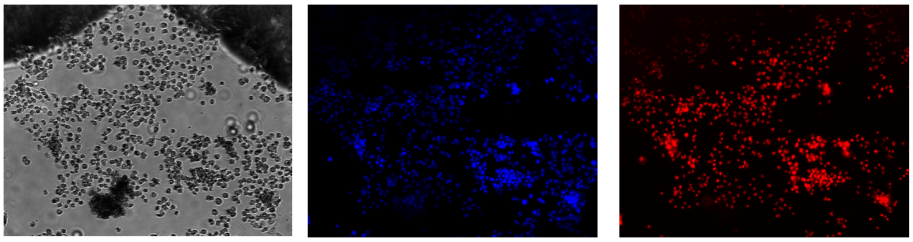

Figure 6.13: In the center of the irradiation spot, one day after irradiation. DIC image to the left, Hoechst stain in the middle and PI stain to the right.

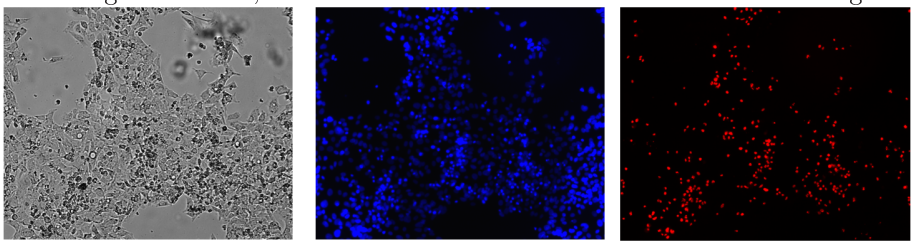

Figure 6.14: Close to (1 cm from) the irradition spot, one day after irradiation. DIC image to the left, Hoechst stain in the middle and PI stain to the right.

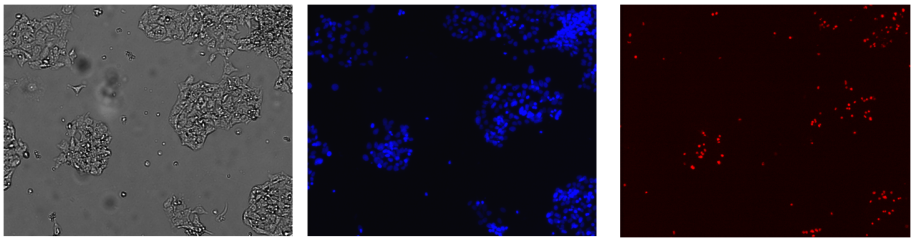

Figure 6.15: At the periphery of the Petri dish, 5 cm from the irradiation spot, one day after irradiation. DIC image to the left, Hoechst stain in the middle and PI stain to the right.

in Paper IV, α_1m was found to significantly reduce the amount of dead cells in both the irradiation center and the peripheries of the cell dish. In the irradiation center, α_1m reduced the amount of dead cells by about 50% and in the peripheries with about 100%, i.e. the cell death decreased down to the same level as in the cells in control dishes (dishes that were not irradiated). The results show that α_1m has a cell-protective effect against alpha particle-induced

cell death.

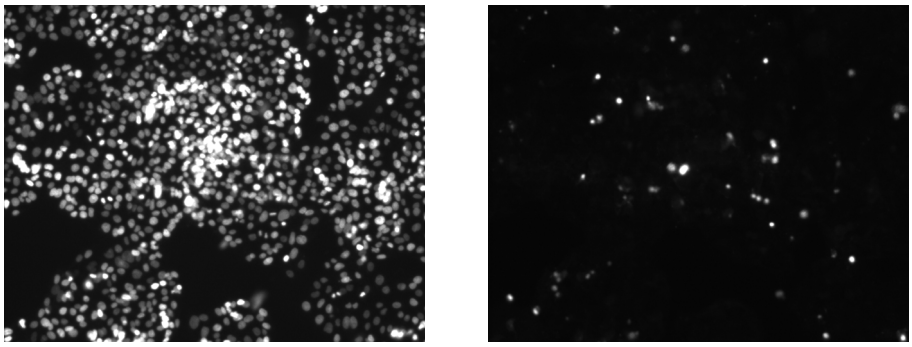

Figure 6.16: Cells cultured, after irradiation, in medium containing α_1m. In the center of the irradiation spot, one day after irradiation. Hoechst stain to the left and PI stain to the right.

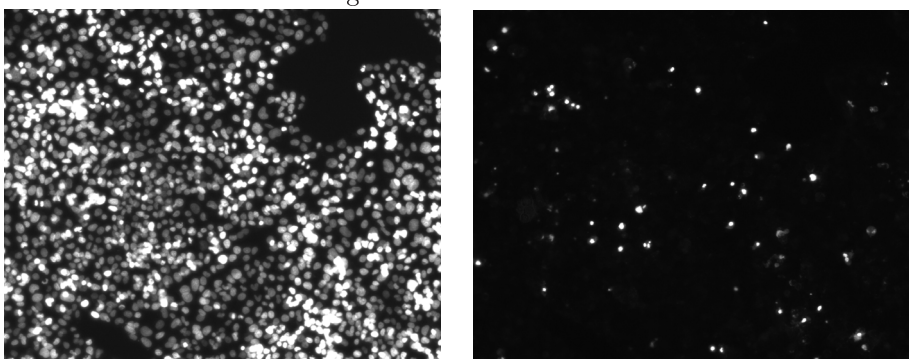

Figure 6.17: Cells cultured, after irradiation, in medium containing α_1m. At the periphery of the Petri dish, far away from the irradiation spot, one day after irradiation. Hoechst stain to the left and PI stain to the right.

6.4 Outlook

Many interesting and important issues regarding HepG2 cells, bystander effects and the effects of α_1-microglobulin remain to be investigated. Firstly, the alpha particle experiments on cells cultured on the patterned cell substrates that, due to lack of time, unfortunately could not be carried out by the time of printing of this thesis should be performed. The aim of this is to further investigate the

pathways of the bystander effect and the effects of α_1-microglobulin.

Planned experiments include measurement of the amount of apoptotic cells following irradiation, using Caspase-3. Also, cell viability after irradiation will be investigated, by measuring the release of lactate dehydrogenase (LDH) into the cell culture. Furthermore, DNA repair of genes is intended to be studied by measuring formation of γH2AX foci in irradited cell cultures. The open question of whether irradiation can induce upregulation of α_1-microglobulin should also be examined, by measuring the messenger-RNA expression of α_1-microglobulin using realtime PCR.

An obvious improvement to the alpha particle experiments would be to use a "simpler" alpha source, for example, one with only one type of decay (i.e. no competing beta decays) and only one decay energy. This would improve the dose calculation by reducing the uncertainty in the LET value. Further improvements could include an improved mask arrangement so as to reduce the collimator size and the beam spreading, among other things. The natural development and logical next step is to switch from experiments using sources to particle microprobe experiments, on cells in both regular Petri dishes as well as patterned cell substrates.

Another interesting development would be to examine induced oxidation in a cell culture, using enzyme-linked immunosorbent assay (ELISA). This would, however, introduce possible obstacles into microprobe experiments, as the ELISA plate would stop the beam completely due to its thickness, meaning that a pre-cell detector would be needed to determine the dose. However, one type of pre-cell detector has been investigated in this thesis, with promising results. Additionally, the ELISA plates do not fit the present sample stage, a minor problem that will also have to be solved.

Chapter 7

Irradiation of tardigrades

One kind of animal that walks, or rather lumbers, the face of the Earth is so small that you are unlikely ever to encounter one, although they live everywhere. They are so tough that they can endure drought, heat, cold close to absolute zero, pressures several orders of magnitude lower than normal air pressure, and 1000 times more ionizing radiation than a human being. Why they are so resistant to various stresses and strains is still not known, although their existence and remarkable qualities have been known since the 1700's. Regarding their radiation tolerance, using a nuclear microprobe to irradiate them and studing their survival is a way of finding out more about how they can withstand 1000 times the lethal dose to a human. The results of these proton microprobe investigations can be found in Paper V.

7.1 Tardigrada

The members of the phylum Tardigrada, in English also known as "water bears" or "moss piglets" (in Swedish *björndjur*), of which about 1000 species are known, are found basically everywhere on planet Earth. Ninety percent of the species are found in fresh water, while ten percent are marine, and they can be found truly everywhere, from the ocean floors to the high mountain tops, and from the tropics to the poles. Tardigrades are not particular about their habitat — their only requirement is liquid water, at least seasonally.

These invertebrate animals are small, usually less than 1 mm long, and have four pairs of thick, unjointed limbs — each of the eight limbs usually has four to eight claws. The body is covered by a cuticle, i.e. an outer, noncellular layer, containing chitin, proteins and lipids, and they come in a variety of colours — from transparent to black. They lack circulatory as well as respiratory systems, but they do have a brain and a nervous system, as well as a gut [81]. When

their stomach is full, this can be seen under a light microscope as a dark area inside the animal. In Figures 7.1 and 7.2 images of a hydrated and a dehydrated tardigrade, respectively, can be seen. The following four figures, 7.3-7.6, show TEM images of a tardigrade, including enlarged images of various parts of the body.

Figure 7.1: Hydrated tardigrade, photo: K. Ingemar Jönsson

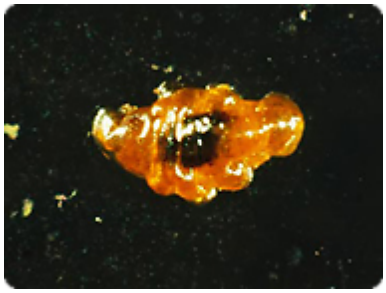

Figure 7.2: Dehydrated tardigrade, photo: K. Ingemar Jönsson

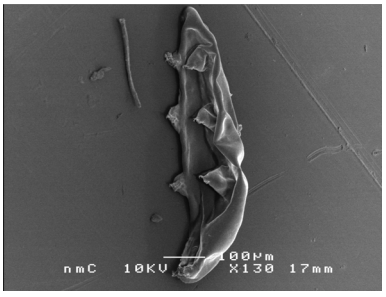

Figure 7.3: Tardigrade, the whole body is shown

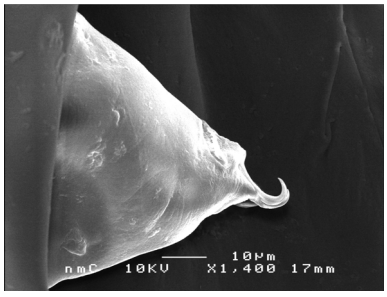

Figure 7.4: Tardigrade, one claw on one of the legs

Tardigrades are suctorial feeders and are equipped with a buccal-pharyngeal apparatus, a feeding apparatus with two sharp stylets, i.e. stiff needle-like organs, and a muscular pharynx, which they use to pierce the cells of their food and suck out the fluids on which they feed. Most tardigrade species feed on plant material, but a few are carnivores. Tardigrades can reproduce in a variety of ways. Normally, a population consists of both males and females and reproduction is sexual, however, populations without males have also been reported, in which case, the development of eggs without fertilization is presumed to be a possibility. Female tardigrades lay 1-30 eggs at a time, and the juvenile tardigrades hatch from these eggs [81].

Figure 7.5: Tardigrade, claws on two legs — probably the hind legs

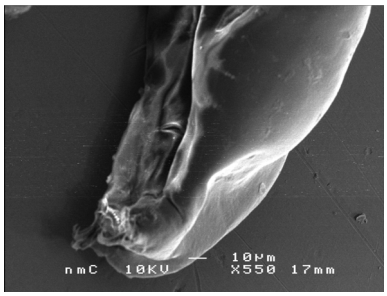

Figure 7.6: Tardigrade, one of the legs with claws

The reason why tardigrades can adapt to almost any hostile environment is their ability to form a "tun", when conditions become unfavourable. Tun formation involves longitudinal contraction of the body together with the limbs being folded inwards, so that the body takes on a constricted, cylindrical shape. When tun formation is complete, all metabolism shuts down, and the relative humidity can decrease down to 0%, causing further desiccation of the tardigrade without killing the animal. In this cryptobiotic state, the tardigrade can survive for an extended period of time until conditions improve and the animal can return to life [81].

Four different cryptobiotic states exist, each defined by the extreme environment that initiates it [81, 82]. Anhydrobiosis is initiated by desiccation and results in the almost complete loss of water from the body, cryobiosis is initiated by a reduction in temperature and means an ordered freezing of the water within the cells. Osmobiosis is initiated by a decrease in water potential due to increased solute concentration in the surrounding solution, but the process by which osmobiosis occurs is not yet understood. Anoxybiosis is initiated by a reduction in oxygen tension. The first three processes may be difficult to tell apart at the organism level, as the entry into the cryptobiotic state may in fact involve more than one of these processes, for example low temperatures will also have a desiccating effect on the organism.

7.2 Experimental approach

In the proton irradiation experiments carried out at the Lund NMP, which are described below, only dehydrated animals, i.e. tardigrades that have entered the cryptobiotic state and are thus "unliving", have been used. A study of the viability of the tardigrades after irradiation in vacuum compared with irradiation in air revealed no difference in viability. Thus, the decision was made

to carry out the main dose-viability experiments in vacuum. Based on earlier survival studies (following alpha particle irradiation) of another tardigrade species, *Milnesium tardigradum* [83], it was decided to expose the tardigrades to nine doses between 500 Gy and 15,000 Gy, i.e. a total of nine experimental groups.

7.2.1 Sample preparation

The tardigrades *Richtersius coronifer* were collected on a heath called *Alvaret* on the island of Öland, Sweden, by collecting pieces of the moss on which the animals live, from the stone walls. The animals were extracted from the moss and then dehydrated, to ensure that they entered the cryptobiotic state. This procedure is described in detail in Paper V. The dehydrated animals were prepared for proton irradiation by mounting five animals at a time on a specially designed backing and covering them with a Mylar foil. After irradiation, the animals were then rehydrated in tap water and their viability investigated. Viable tardgirades were defined as those showing coordinated leg motion.

7.2.2 Irradiation protocol

The number of animals irradiated at each dose was based on earlier, related studies [83, 84]. Two groups of 15 animals were irradiated at each dose. In addition, a control group of 2 $\times$ 15 animals was exposed to vacuum only for the same period of time as the experimental groups (about 30-45 minutes).

Protons with an energy of 2.55 MeV were used for the irradiation experiments. The energy loss in the 6 μm thick Mylar covering the animals is 100 keV; thus, the energy of the protons after passing through the Mylar was 2.45 MeV. The initial calculation of the dose per proton was carried out using the following relationship:

$$Dose[Gy = J/kg] = LET[eV/\mu m] \cdot 1.602 \cdot 10^{-19}[J/eV] \cdot \frac{targetthickness[\mu m]}{targetmass[kg]} \tag{7.1}$$

The software SRIM [13] was used to calculate the linear energy transfer to the tardigrades. The tardigrades were modelled as organic matter, with a density of 1 g/cm^3. At 2.45 MeV, the LET of the protons is 14 keV/μm. The range of 2.45 MeV protons in organic matter, 107 μm, is less than the thickness of the animals (250 μm), which means that the protons are completely stopped in the tardigrade. Thus, the product of LET $\times$ target thickness can be replaced by the full energy of the protons. The dry mass of the animals is 2-3 μg, and a value of 3 μg was used in the calculations. Given the dose per proton, the number of protons required to deliver the desired dose could be calculated;

this number was then converted to the corresponding charge that needed to be delivered.

The tardigrades were irradiated with a defocused proton beam, with a beam size of approximately 150 μm $\times$ 150 μm. This beam size was considered to be large enough to roughly match the area of the tardigrade body, but still small enough that beam does not pass around the body and is lost. By measuring the beam current, i.e. charge per unit time, during and between irradiation, the appropriate irradiation time could be determined. The beam current was measured just before the target chamber using an amp meter as well as on the sample using an electrometer. The beam blanker was used to direct the predetermined charge onto the tardigrade sample; the irradiation time was 0.1-1 s.

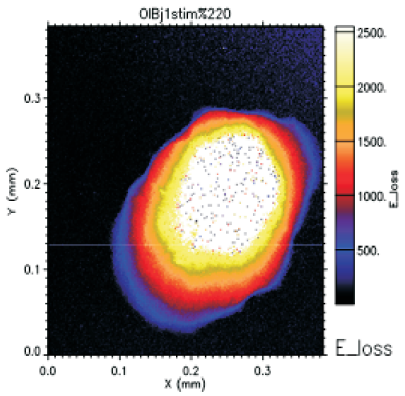

Figure 7.7: STIM map of dehydrated tardigrade, showing how the energy loss varies over the animal.

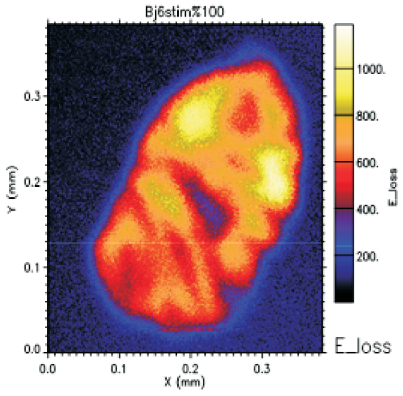

Figure 7.8: STIM map of freeze-dried tardigrade, showing how the energy loss varies over the animal.

To confirm the assumption that the dehydrated tardigrades are thick enough to completely stop the 2.55 MeV proton beam, and thus validate the dose calculation described, the energy loss of 2.55 MeV protons in dehydrated and freeze-dried tardigrades was measured using STIM. The data was analysed using the software GeoPIXE [76, 85]. Results from these STIM analyses are shown in Figures 7.7-7.9. The STIM analysis revealed a considerable difference in thickness between the freeze-dried and the dehydrated animals, as expected. The longitudinal contraction of the dehydrated tardigrade is evident; this sample is much thicker and more spherically shaped than the freeze-dried specimen, which is considerably thinner and flatter.

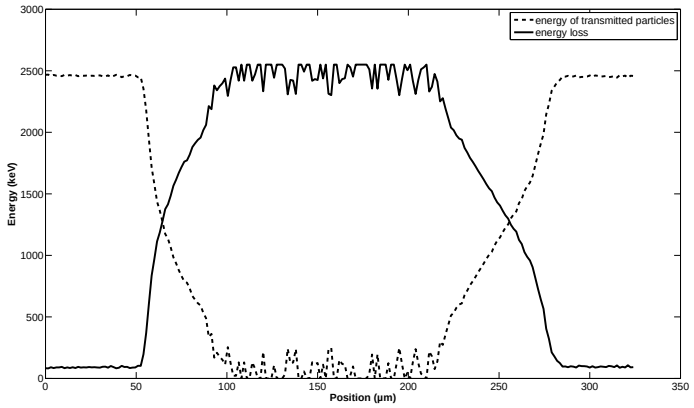

Figure 7.9: Traverse across the dehydrated tardigrade, showing the remaining energy after penetration of the animal as well as the energy loss in the animal.

Based on the STIM analysis, it was concluded that the thickness of a dehydrated tardigrade at its centre is greater than the range of the protons. However, the thickest portion of the animal is generally somewhat smaller than the defocused beam size, meaning that some of the protons will pass the animal without depositing all of their energy. This means that a correction of the absorbed dose should be made — based on the samples analysed, a correction of 10 % was sufficient to ensure that the LD50 value was not overestimated. STIM was also used to determine the areal mass density in the tardigrades. Figure 7.10 shows how the areal mass density varies over the body of a freeze-dried tardigrade (the same sample as is shown in Figure 7.8).

7.3 Dose-viability relationship after proton irradiation

After rehydration, the tardigrades were inspected three times over the course of the first two days: 4 hours, 24 hours and 48 hours after rehydration. The resulting viability curve as a function of dose revealed that the LD50 dose is 10,200 Gy, and that virtually all the animals were dead after receiving a dose of 12,000 Gy.

A major difference between this study and the previous publications, using gamma rays [83, 84] or 50 MeV alpha particles [83], is that in this case almost the full energy of the protons is deposited in the animals, i.e. the protons reach

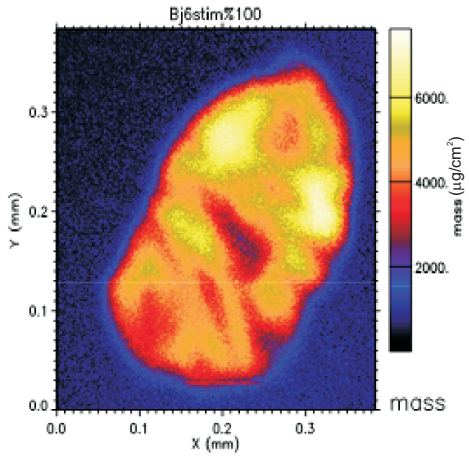

Figure 7.10: STIM map of freeze-dried tardigrade, showing how the areal mass density varies over the animal.

the end of their range. However, the LET of the protons in this case, 14.15 keV/μm, is comparable to the LET of 50 MeV alpha particles, 16.3 keV/μm. In the case of gamma rays and high-energy alpha particles, the range of the particles by far exceeds the thickness of the animals. Figures 7.11 and 7.12 illustrate the beam straggling and the energy loss, or stopping, of 2.45 MeV protons (Figure 7.11) and 50 MeV alpha particles (Figure 7.12) while travelling through 250 μm of water (chosen to resemble the organic matter). As can be seen in these figures, the protons spread considerably more as they penetrate the water and reach the end of their range. The fact that the protons deposit more energy per unit path length as they approach the end of their range must be taken into consideration (cf. the Bragg curve, Figure 2.5), which in this case means that most of the energy will be deposited on the opposite side to that where the beam enters the animal. As it is not known whether tardigrades have any parts that are more or less sensitive to radiation, the orientation of the animal on the backing could make a difference, i.e. which part of the animal receives more radiation.

It is still not known whether the tardigrade's ability to tolerate ionizing radiation is due to the fact that they do not suffer any DNA damage or whether they are very efficient in repairing DNA damage. No study of tardigrade DNA damage caused by ionizing radiation has yet been published. However, a study

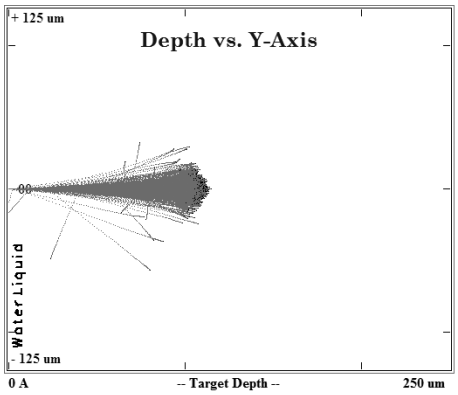

Figure 7.11: 2.45 MeV protons penetrating 250 μm of water: Depth vs. distance

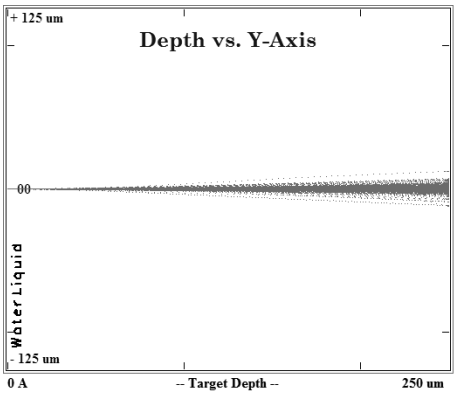

Figure 7.12: 50 MeV alpha particles penetrating 250 μm of water: Depth vs. distance

involving gel electrophoresis analysis of DNA damage in bdelloid rotifers (a desiccation-tolerant class of rotifers called *"hjuldjur"* in Swedish), after gamma irradiation [86] has shown that bdelloid rotifers do in fact suffer the same amount of double strand breaks in DNA as radio-sensitive organisms, and that the number of DSBs is directly proportional to the dose. However, this class of rotifers has an enhanced capacity to scavenge reactive molecular species caused by the radiation, so that the cellular components that are essential for the repair of damaged DNA are protected. It was also suggested in the same publication that the bdelloid rotifers are not so much radiation-tolerant as very well adapted to the damage, most probably including DNA damage, that they suffer during periods of severe desiccation — DNA damage caused by desiccation is then repaired upon rehydration of the animals.

7.4 Ion beam analysis of tardigrades

In the search for a possible explanation of the extreme radiation tolerance of tardigrades, the elemental composition of the animals was investigated using qualitative PIXE analysis. Manganese, or rather the ratio of manganese to iron, has previously been shown to be related to dehydration tolerance and radioresistance (γ-radiation) in the bacteria *Deinococcus radiodurans* [87]. These radioresistant bacteria have been shown to contain 300 times more manganese and 3 times less iron than related, but radiosensitive bacteria. *Deinococcus radiodurans* cells were analysed using an XRF microprobe and the analysis revealed that Mn was distributed throughout the cell while Fe was present mainly

outside the cytoplasm [87].

The presence and distribution of different elements in the animals was investigated with micrometre lateral resolution and the data analysed using the GeoPIXE software [76]. In the dehydrated animals (a total of four animals were analysed), sulphur, chlorine, potassium, calcium, iron and a small amount of phosphorus were present. In the freeze-dried animals, i.e. animals that have not entered the cryptobiotic state, (a total of five animals were analysed), sulphur, potassium, calcium, iron, phosphorus and low amounts of chlorine were present. Elemental maps of dehydrated and freeze-dried tardigrades are shown in Paper V. Differences within the two groups are quite small. When comparing the dehydrated and freeze-dried animals, the distribution of all of the above mentioned elements except potassium and calcium were found to be significantly different. Calcium is known to be found in the mouth and the claws of the animals, as is particularly visible in the Ca map in Figure 7.13. None of the dehydrated animals analysed revealed any particular level or distribution of manganese. Of the freeze-dried animals analysed, only one appears to contain an amount of manganese that is clearly distinguishable from the background, see Figure 7.14. It does appear that dehydration of a tardigrade causes some redistribution of elements, especially of sulphur and chlorine — from the even distribution throughout the body in a hydrated animal, to a localization close to the surface in the dehydrated state. It is, however, difficult to draw a definite conclusion, due to the fact that not all animals are oriented in the same way on the backing, meaning that it is difficult to judge whereto exactly the elements have wandered.

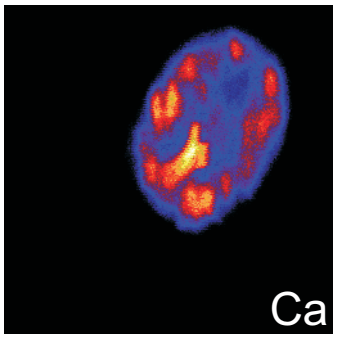

Figure 7.13: Calcium map of a dehydrated tardigrade. Calcium maps the mouth and claw structures of the animal. The size of the map is 384 μm $\times$ 384 μm.

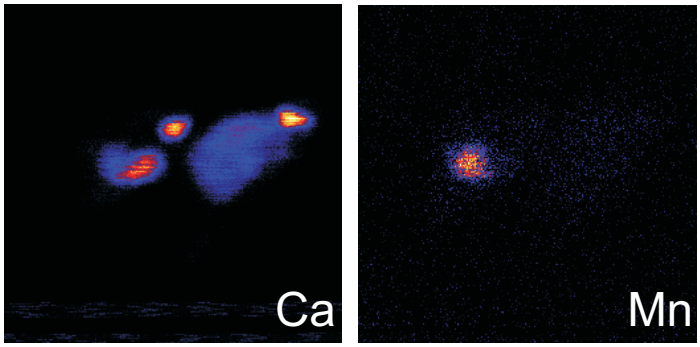

Figure 7.14: Calcium and manganese maps of two freeze-dried tardigrades. The size of the map is 576 μm $\times$ 576 μm.

7.5 Outlook

In future proton microbeam irradiation experiments, the irradiation strategy could be altered in different ways. One alternative would be to irradiate only the smaller area in the centre of the tardigrade that completely stops the beam — this would, however, increase to risk of missing a potentially radiation sensitive section of the tardigrade. Another option would be to use the proton beam energy as a parameter in the experiments. This way, the penetration depth could be changed, so that, for example, only the surface of the tardigrade would be irradiated.

Studies must be conducted to ascertain whether the same efficient DNA repair mechanism that seems to be pivotal in the radiation tolerance of bdelloid rotifers, is also the key to the radiation tolerance of the tardigrades. If it is not, what does govern its tolerance to ionizing radiation? The application of PIXE analysis in the quest for an answer as to why the tardigrades are so radiation-tolerant should be further explored. Future studies should also be directed towards establishing where in the tardigrade the irradiation tolerance is located, and whether specific parts, or even proteins or enzymes, of the animal have to be irradiated in order to kill it. Different parts of a tardigrade can be selected for irradiation with varying doses using a microprobe, or a low-current beam could be scanned over the animal. Hydrated tardigrades should also be irradiated, to find the LD50 value in this state.

Tardigrades could perhaps be used as biological markers, in investigations of pollutants and heavy metals, for example. As these animals can be found almost everywhere, populations from different environments could be gathered and compared with respect to their elemental content. Another line of inves-

tigation could be to compare tardigrades living close to a nuclear power plant with those living far away (in a "background area"), to determine whether they differ in radiation tolerance — as the group living in the vicinity of the power plant possibly have received a "priming dose", it could be investigated if adaptive responses can be identified.

Chapter 8

Acknowledgements

First and foremost I would like to express my deepest gratitude to my main supervisor Dr. Jan Pallon, for inspiring me to start my Ph.D. studies, for his tirelss support over the years, for having faith in me when I didn't, for celebrating with me when times were good and for picking me up when I fell — I truly could not have wished for a better supervisor.
I would also like to thank the two people who I have adopted as my assistant supervisors — Professor Per Kristiansson and Dr. Mikael Elfman. Thank you Per, for lots of help in the lab as well as with the obstacles of bureaucracy — always with "mer morot än piska"... And thank you Mikael, for all your help in the lab, for your company during odd hours and for all the fun and games.
The other members of the Microprobe Group — past and present — also deserve a sincere thank you. Thanks to Christer Nilsson, my fellow CELLION Ph.D. student Natalia Arteaga Marrero and Dr. Marie Wegdén.
My most long-lived office mates, Marie Sydoff and Natalia Arteaga Marrero, deserve thanks for their day-to-day company, the smalltalk, the philosophising about life and everything else.
For the daily laughs at work, I would also like to thank the rest of the people working at the Division of Nuclear Physics. Not only has it been a pleasure to go to work (almost) every day, thanks to things like the *fika* at three, but many of you have also helped me with a little of everything over the years — answering questions (whether they were physics related or not), showing me around in the chemistry lab, providing me with the right form to fill in, and more... Thank you to all of you (*"ingen nämnd, ingen glömd"*).
My collaborators, Dr. Göran Thungström, Professor Bo Åkerström, Magnus Olsson, Dr. Johan Nilsson and Dr. Ingemar Jönsson, have all been a tremendous help at various stages of this work — thank you all.
I would like to thank Professor Tilman Butz for inviting me to Leipzig as a Marie Curie fellow. I would also like to thank the other members of the Nuclear

Solid State Physics group in Leipzig, who were helpful.
The people who helped me improve my work by reading and commenting on this thesis definitely deserve thanks. Marie, Ingemar, Magnus, Per and of course Jan — thank you all.
Although I enjoy my life in nuclear physics, I am grateful that I have a life outside nuclear physics as well — for this, I wish to thank my non-nuclear friends. Thank you for not forgetting me while I was in Germany (although I am terrible at keeping in touch...), for being my home away from home when I didn't have a home in Sweden, and for all the little things — the cookie baking, the movies and card games...
My father also deserves a huge thank you for holding the fort while I was in Germany — for helping me move, for the regular packages in the mail and for taking care of Taxen. Last but not least, I have three truly great brothers, Kristian, Henrik and Johan. You have been the best companions for so many years — I'm very happy to have you! *Kram på er!*

Bibliography

[1] E.J. Hall, A.J. Giaccia, *Radiobiology for the radiologist*, Lippincott Williams & Wilkins (2006).

[2] K.M. Prise, M. Folkard, B.D. Michael, *A review of the bystander effect and its implications for low-dose exposure*, Radiation Protection Dosimetry **104** (2003) 347-355.

[3] M. Folkard, K.M. Prise, A.G. Michette, B. Vojnovic, *The use of radiation microbeams to investigate the bystander effect in cells and tissues*, Nuclear Instruments and Methods in Physics Research A **580** (2007) 446-450.

[4] C.R. Geard, D.J. Brenner, G. Randers-Pehrson, S.A. Marino, *Single-particle irradiation of mammalian cells at the Radiological Research Accelerator Facility: induction of chromosomal changes*, Nuclear Instruments and Methods in Physics Research B **54** (1991) 411-416.

[5] M. Folkard, K.M. Prise, B. Vojnovic, H.C. Newman, M.J. Roper, K.J. Hollis, B.D. Michael, *Conventional and microbeam studies using low energy charged particles relevant to risk assessment and the mechanics of radiation action*, Radiation Protection Dosimetry **61** (1995) 215-218.

[6] B.E. Fischer, M. Cholewa, H. Nogushi, *Some experiences on the way to biological single ion experiments*, Nuclear Instruments and Methods in Physics Research B **181** (2001) 60-65.

[7] A.W. Bigelow, D.J. Brenner, G. Garty, G. Randers-Pehrson, *Single-particle/single-cell ion microbeams as probes of biological mechanisms*, IEEE Transactions on Plasma Science **36** (2008) 1424-1431.

[8] M. Folkard, K. Prise, G. Schettino, C. Shao, S. Gilchrist, B. Vojnovic, *New insights into the cellular response to radiation using microbeams*, Nuclear Instruments and Methods in Physics Research B **231** (2005) 189-194.

[9] <http://cellion.ifj.edu.pl/>

[10] W.R. Leo, *Techniques for Nuclear and Particle Physics Experiments: A How-to Approach.*, Springer-Verlag, Berlin; New York (1994).

[11] F.A. Cucinotta, H. Nikjoo, D.T. Goodhead, *The effects of delta rays on the number of particle-track traversals per cell in laboratory and space exposures*, Radiation Research **150** (1998) 115-119.

[12] V. Auzelyte, *Direct writing with an MeV proton beam: Development and applications*, Doctoral thesis, Lund University (2006).

[13] J.F. Ziegler, *SRIM 2008, Version SRIM-2008.03.* Available from: <http://www.srim.org>.

[14] U.A.S. Tapper, K.G. Malmqvist, *Analysis, imaging and modification of microscopic specimens with accelerator beams*, Analytical Chemistry **63** (1991) 715-725.

[15] J.C. Overley, R.M.S. Schofield, J.D. Macdonald, H.W. Lefevre, *Energy-loss image formation in scanning transmission ion microscopy*, Nuclear Instruments and Methods in Physics Research B **30** (1988) 337-341.

[16] S.A.E. Johansson, J.L. Campbell, *PIXE: A novel technique for elemental analysis*, John Wiley & Sons (1988).

[17] S. Johansson, P. Kristiansson, K. Malmqvist, S. Tapper, *Introduktion till Kärnfysiken*, Femte reviderade upplagan, v.5.2, KFS AB, Lund 2000.

[18] G.I. Johansson, J. Pallon, K.G. Malmqvist, K.R. Akselsson, *Calibration and long-term stability of a PIXE set-up*, Nuclear Instruments and Methods in Physics Research B **181** (1981) 81-88.

[19] A. Shariff, C. Nilsson, V. Auzelyte, M. Elfman, P. Kristiansson, K. Malmqvist, J. Pallon, M. Wegden, *The Lund Nuclear Microprobe sub-micron set-up. Part II: Beam line, focusing system and scanning*, Nuclear Instruments and Methods in Physics Research B **231** (2005) 7-13.

[20] A. Shariff, V. Auzelyte, M. Elfman, P. Kristiansson, K. Malmqvist, C. Nilsson, J. Pallon, M. Wegden, *The Lund Nuclear Microprobe sub-micron set-up. Part I: Ion optics calculation*, Nuclear Instruments and Methods in Physics Research B **231** (2005) 1-6.

[21] Technisches Büro T. Fischer, Am Berg 9, D-64372 Ober-Ramstadt, Germany

[22] V. Auzelyte, M. Elfman, P. Kristiansson, K. Malmqvist, L. Wallman, C. Nilsson, J. Pallon, A. Shariff, M. Wegdén, *The beam blanking system for microlithography at Lund Nuclear Microprobe*, Nuclear Instruments and Methods in Physics Research B **219-220** (2004) 485-489.

[23] M. Elfman, J. Pallon, V. Auzelyte, P. Kristiansson, K. Malmqvist, C. Nilsson, A. Shariff, M. Wegdén, *The Lund Nuclear Microprobe sub-micron set-up. Part III: Sample stage, optical imaging and detector configuration in the experimental chamber*, Nuclear Instruments and Methods in Physics Research B **231** (2005) 14-20.

[24] A. Shariff, P. Kristiansson, V. Auzelyte, M. Elfman, K.G. Malmqvist, C. Nilsson, J. Pallon, M. Wegden, *Characterization of a new large area HPGe X-ray detector for low beam current application*, Nuclear Instruments and Methods in Physics Research B **219-220** (2004) 494-498.

[25] N. Arteaga-Marrero, J. Pallon, M.G. Olsson, V. Auzelyte, M. Elfman, P. Kristiansson, K. Malmqvist, C. Nilsson, M. Wegdén, *The new Cell Irradiation Facility at the Lund Nuclear Probe*, Nuclear Instruments and Methods in Physics Research B **260** (2007) 91-96.

[26] N. Arteaga-Marrero, M.G. Olsson, J. Pallon, B. Åkerström, M. Elfman, P. Kristiansson, C. Nilsson, Ch. Nilsson, M. Wegdén, *Oxidative effects related to proton irradiation in $HepG_2$ cell line at the Lund Nuclear Probe*, presented at ICRR 2007, San Francisco, USA, July 2007

[27] B.E. Fischer, M. Heiß, M. Cholewa, *About the art to shoot with single ions*, Nuclear Instruments and Methods in Physics Research B **210** (2003) 285-291.

[28] M. Folkard, G. Schettino, B. Vojnovic, S. Gilchrist, A.G. Michette, S.J. Pfauntsch, K.M. Prise, B.D. Michael, *A focused ultrasoft X-ray microbeam for targeting cells individually with submicrometer accuracy*, Radiation Research **156** (2001) 796-804.

[29] E.H. Kim, G.M. Sun, M. Jang, *An electron microbeam cell-irradiation system at KIRAMS: performance and preliminary experiments*, Radiation Protection Dosimetry **122** (2006) 297-300.

[30] M. Sowa Resat, W.F. Morgan, *Microbeam developments and applications: A low linear energy transfer perspective*, Cancer and Metastasis Reviews **23** (2004) 323-331.

[31] M. Wegdén, M. Elfman, P. Kristiansson, N. Arteaga Marrero, V. Auzelyte, K.G. Malmqvist, C. Nilsson, J. Pallon, *A pre-target charge measurement system for "pixel-by-pixel" normalisation*, presented at ICNMTA 2006, Singapore, July 2006

[32] M. Folkard, B. Vojnovic, K.J. Hollis, A.G. Bowey, S.J. Watts, G. Schettino, K.M. Prise, B.D. Michael, *A charged particle microbeam: II. A single-particle micro-collimation and detection system*, International Journal of Radiation Biology, **72** (1997) 387-395

[33] M. Folkard, B. Vojnovic, K.M. Prise, A.G. Bowey, R.J. Locke, G. Schettino, B.D. Michael, *A charged particle microbeam: II. Development of an experimental system for targeting cells individually with counted particles*, International Journal of Radiation Biology, **72** (1997) 375-385

[34] Ph. Barberet, A. Balana, S. Incerti, C. Michelet-Habchi, Ph. Moretto, Th. Pouthier, *Development of a focused charged particle microbeam for the irradiation of individual cells*, Review of Scientific Instruments **76** (2004) 015101.

[35] G. Randers-Pehrson, C.R. Geard, G. Johnson, C.D. Elliston, D.J. Brenner, *The Columbia University Single-Ion Microbeam*, Radiation Research **156** (2001) 210-214.

[36] M. Folkard, B. Vojnovic, S. Gilchrist, K.M. Prise, B.D. Michael, *The design and application of ion microbeams for irradiating living cells and tissues*, Nuclear Instruments and Methods in Physics Research B **210** (2003) 302-307.

[37] M. Heiß, B.E. Fischer, B. Jakob, C. Fournier, G. Becker, G. Taucher-Scholz, *Targeted Irradiation of Mammalian Cells Using a Heavy-Ion Microprobe*, Radiation Research **165** (2006) 231-239.

[38] T. Funayama, S. Wada, Y. Kobayashi, H. Watanabe, *Irradiation of Mammalian Cultured Cells with a Collimated Heavy-Ion Microbeam*, Radiation Research **163** (2005) 241-246.

[39] W. Polak, O. Veselov, J. Lekki, Z. Stachura, M. Zazula, R. Ugenskiene, M. Polak, J. Styczen, *Irradiating single cells using Cracow microprobe facility*, Nuclear Instruments and Methods in Physics Research B **249** (2006) 743-746.

[40] T. Reinert, A. Fiedler, J. Skopek, J. Tanner, J. Vogt, T. Butz, *Single ion bombardment of living cells at LIPSION*, Nuclear Instruments and Methods in Physics Research B **219-220** (2004) 77-81.

[41] S. Gerardi, G. Galeazzi, R. Cherubini, *A Microcollimated Ion Beam Facility for Investigations of the Effects of Low-Dose Radiation*, Radiation Research **164** (2005) 586-590.

[42] J.C. Yanch, *Development of a Charged Particle Microbeam for Targeted and Single Particle Subcellular Irradiation*, Technical Report DOE/ID13643, Massachusetts Institute of Technology (US), 2004.

[43] K.D. Greif, H.J. Brede, D. Frankenberg, U. Giesen, *The PTB single ion microbeam for irradiation of living cells*, Nuclear Instruments and Methods in Physics Research B **217** (2004) 505-512.

[44] A. Hauptner, S. Dietzel, G.A. Drexler, P. Reichart, R. Krücken, T. Cremer, A.A. Friedl, G Dollinger, *Microirradiation of cells with energetic heavy ions*, Radiation and Environmental Biophysics **42** (2005) 237-245.

[45] K.J. Kirkby, G.W. Grime, R.P. Webb, N.F. Kirkby, M. Folkard, K. Prise, B. Vojnovic, *A scanning focussed vertical ion nanobeam: A new UK facility for cell irradiation and analysis*, Nuclear Instruments and Methods in Physics Research B **260** (2007) 97-100.

[46] Y. Kobayashi, T. Funayama, S. Wada, M. Taguchi, H. Watanabe, *Irradiation of single mammalian cells with a precise number of energetic heavy ions — Applications of microbeams for studying cellular radiation response*, Nuclear Instruments and Methods in Physics Research B **210** (2003) 308-311.

[47] G. Dollinger, V. Hable, A. Hauptner, R. Krucken, P. Reichart, A.A. Friedl, G. Drexler, T. Cremer, S. Dietzel, *Microirradiation of cells with energetic heavy ions*, Nuclear Instruments and Methods in Physics Research B **231** (2005) 195-201.

[48] K.S. Krane, *Introductory nuclear physics*, John Wiley & Sons, Inc. (1988).

[49] E.J. Hall, T.K. Hei, *Genomic instability and bystander effect induced by high-LET radiation*, Oncogene **22** (2003) 7034-7042.

[50] Belli, *RBE-LET relationship for the survival of V79 cells irradiated with low energy protons*, International Journal of Radiation Biology **55** (1989) 93-104.

[51] K.M. Prise, M. Folkard, B.D. Michael, *Radiation-induced bystander and adaptive responses in cell and tissue models*, Dose-Response **4** (2006) 263-276.

[52] B.E. Lehnert, R. Iyer, *Exposure to low-level chemicals and ionizing radiation: reactive oxygen species and cellular pathways*, Human & Experimental Toxicology **21** (2002) 65-69.

[53] K.M. Prise, O.V. Belyakov, H.C.Newman, S. Patel, G. Schettino, M. Folkard, B.D. Michael, *Non-targeted effects of radiation: bystander responses in cell and tissue models*, Radiation Protection Dosimetry **99** (2002) 223-226.

[54] O.V. Belyakov, E.J. Hall, S.A. Marino, G. Randers-Pehrson, D.J. Brenner, *Studies of bystander effects in artificial human 3D tissue systems using a microbeam irradiation*, in Proceedings of the 11th International Congress of the International Radiation Protection Association, IRPA11, Madrid, Spain, 2004.

[55] C. Shao, Y. Furusawa, Y. Kobayashi, T. Funuyama, S. Wada, *Bystander effect induced by counted high-LET particles in confluent human fibroblasts: a mechanistic study*, The FASEB Journal **17** (2003) 1422-1427.

[56] F.M. Lyng, C.B. Seymour, C. Mothersill, *Initiation of apoptosis in cells exposed to medium from the progeny of irradiated cells: A possible mechanism for bystander-induced genomic instability?*, Radiation Research **157** (2002) 365-370.

[57] W.F. Morgan, M.B. Sowa, *Non-targeted bystander effects induced by ionizing radiation*, Mutation Research **616** 2007 159-164.

[58] C. Shao, Y. Furusawa, Y. Kobayashi, T. Funayama, *Involvement of gap junction intercellular communication in the bystander effect induced by broad-beam or microbeam heavy ions*, Nuclear Instruments and Methods in Physics Research B **251** (2006) 177-181.

[59] C. Shao, Y. Furusawa, M. Aoki, H. Matsumoto, K. Ando, *Nitric oxide-mediated bystander effect induced by heavy-ions in human salivary gland tumour cells*, International Journal of Radiation Biology **78** (2002) 837-844.

[60] C. Shao, M. Aoki, Y. Furusawa, *Bystander effect in lymphoma cells vicinial to irradiated neoplastic epithelial cells: nitric oxide is involved*, Journal of Radiation Research **45** (2004) 97-103.

[61] H. Matsumoto, S. Hayashi, M. Hatashita, K. Ohnishi, H. Shioura, T. Ohtsubo, R. Kitai, T. Ohnishi, E. Kano, *Induction of radioresistance by a nitric oxide-mediated bystander effect*, Radiation Research **155** (2001) 387-396.

[62] B.E. Lehnert, E.H. Goodwin, *Extracellular factor(s) following exposure to α particles can cause sister chromatid exchanges in normal human cells*, Cancer Research **57** (1997) 2164-2171.

[63] P.K. Narayanan, E.H. Goodwin, B.E. Lehnert, *α particles initiate biological production of superoxide anions and hydrogen peroxide in human cells*, Cancer Research **57** (1997) 3963-3971.

[64] A. Bishayee, H.Z. Hill, D. Stein, D.V. Rao, R.W. Howell, *Free radical-initiated and gap junction-mediated bystander effect due to nonuniform distibution of incorporated radioactivity in a three-dimensional tissue culture model*, Radiation Research **155** (2001) 335-344.

[65] E.I. Azzam, S.M. de Toledo, J.B. Little, *Direct evidence for the participation of gap junction-mediated intercellular communication in the transmission of damage signals from α-particle irradiated to nonirradiated cells*, Proceedings of the National Academy of Sciences **98** (2001) 473-478.

[66] Hoechst Stains, Invitrogen, Molecular Probes, Inc., <http://probes.invitrogen.com/media/pis/mp21486.pdf>

[67] Propidium Iodide Nucleic Acid Stain, Invitrogen, Molecular Probes, Inc., <http://probes.invitrogen.com/media/pis/mp01304.pdf>

[68] G. Thungström, L. Westerberg, R. Spohr, C. S. Petersson, *Fabrication and characterization of thin ΔE detectors for spectroscopic application*, Nuclear Instruments and Methods in Physics Research A **546** (2005) 312-318.

[69] G.F. Knoll, *Radiation detection and measurement*, John Wiley & Sons, Inc. (1979).

[70] KMax Sparrow software, <http://www.sparrowcorp.com>

[71] R. Siegele, M. Reinhard, D. Prokopovich, M. Ionescu, D.D. Cohen, A.B. Rosenfeld, I.M. Cornelius, A. Wroe, M.L.F. Lerch, A. Fazzi, A. Pola, S. Agosteo, *Characterisation of a ΔE-E particle telescope using the ANSTO heavy ion microprobe*, Nuclear Instruments and Methods in Physics Research B **270** (2007) 270-275.

[72] C. Shao, M. Folkard, B.D. Michael, K.M. Prise, *Bystander signaling between glioma cells and fibroblasts targeted with counted ions*, International Journal of Cancer **116** 2005 45-51.

[73] Goodfellow, <http://www.goodfellow.com>

[74] BD Biosciences Europe, <http://www.bdeurope.com/>

[75] BD Cell-Tak^{TM} Cell and Tissue Adhesive — Instructions for Use, BD Biosciences, <http://www.bdbiosciences.com/docs/Products/cell_environments_and_ECMs/354240.pdf>

[76] GeoPIXE II software, <http://nmp.csiro.au/GeoPIXE.html>

[77] <www.atcc.org>

[78] B. Åkerström, L. Lögdberg, α_1-*Microglobulin*, Chapter 10 in Lipocalins, edited by Bo Åkerström, Niels Borregaard, Darren R. Flower and Jean-Philippe Salier (2006).

[79] M. Folkard, K.M. Prise, B. Vojnovic, *Status of charged particle microbeams for radiation biology*, Journal of Physics: Conference Series **58** (2007) 62-67.

[80] S. Gerardi, *A comparative review of charged particle microbeam facilities*, Radiation Protection Dosimetry **122** (2006) 285-291.

[81] D.R. Nelson, N.J. Marley, *The biology and ecology of lotic Tardigrada*, Freshwater Biology **44** (2000) 93-108.

[82] K.I. Jönsson, *Causes and consequences of excess resistance in cryptobiotic metazoans*, Physiological and Biochemical Zoology **76** (2003) 429-435.

[83] D.D. Horikawa, T. Sakashita, C. Katagiri, M. Watanabe, T. Kikawada, Y. Nakahara, N. Hamada, S. Wada, T. Funayama, S. Higashi, Y. Kobayashi, T. Okuda, M. Kuwabara, *Radiation tolerance in the tardigrade Milnesium tardigradum*, International Journal of Radiation Biology **82** (2006) 843-848.

[84] K.I. Jönsson, M. Harms-Ringdahl, J. Torudd, *Radiation tolerance in the eutardigrade Richtersius coronifer*, International Journal of Radiation Biology **81** (2005) 649-656.

[85] J. Pallon, C.G. Ryan, N. Arteaga Marrero, M. Elfman, P. Kristiansson, E.J.C. Nilsson, C. Nilsson, *STIM evaluation in GeoPIXE to complement the quantitative Dynamic Analysis*, Accepted for publication in Nuclear Instruments and Methods in Physics Research B, Proceedings of the 11th International Conference on Nuclear Microprobe Technology and Applications (2008).

[86] E. Gladyshev, M. Meselson, *Extreme resistance of bdelloid rotifers to ionizing radiation*, Proceedings of the National Academy of Sciences **105** (2008) 5139-5144.

[87] M.J. Daly, E.K. Gaidamakova, V.Y. Matrosova, A. Vasilenko, M. Zhai, R.D. Leapman, B. Lai, B. Ravel, S.-M.W. Li, K.M. Kemner, J.K. Fredrickson, *Protein oxidation implicated as the primary determinant of bacterial radioresistance*, Public Library of Science Biology **5** (2007) 769-779.